Centromeres are dismantled by foundational meiotic proteins Spo11 and Rec8

Haitong Hou[1,2,3,*], **Eftychia Kyriacou**[3,4,*], **Rahul Thadani**[1,3], **Michael Klutstein**[5], **Joseph H. Chapman**[3,6], **Julia Promisel Cooper**[1,2,3]

[1]Department of Biochemistry and Molecular Genetics, University of Colorado Anschutz Medical Campus, 12801 E. 17th Ave, Aurora, CO 80045, Phone 303-724-3203

[3]Former address: Telomere Biology Laboratory, Laboratory of Biochemistry and Molecular Biology, Center for Cancer Research, NCI, NIH, Bethesda, MD 20892

[4]Current address: Swiss Institute for Experimental Cancer Research (ISREC), School of Life Sciences, Ecole Polytechnique Fédérale de Lausanne (EPFL), Lausanne, Switzerland

[5]Chromatin and Aging Research Laboratory, Institute of Dental Science, Hebrew University of Jerusalem PO 12272, Israel 91120

[6]Current address: Single Molecular Biophysics Laboratory, NHLBI, NIH

Abstract

Meiotic processes are potentially dangerous to genome stability and could be disastrous if activated in proliferative cells. Here we show that two key meiosis-defining proteins, the double strand break-forming topoisomerase Spo11 and the meiotic cohesin Rec8, can dismantle centromeres. This dismantlement is normally observable only in mutant cells lacking the telomere bouquet, which provides a nuclear microdomain conducive to centromere reassembly[1]; however, overexpression of Spo11 or Rec8 leads to levels of centromere dismantlement that cannot be countered by the bouquet. Specific nucleosome remodeling factors mediate centromere dismantlement by Spo11 and Rec8. Remarkably, ectopic expression of either protein in proliferating cells leads to mitotic kinetochore loss in both fission yeast and human cells. Hence, while centromeric chromatin has been characterized as extraordinarily stable, Spo11 and Rec8 challenge this stability, and may jeopardize kinetochores in the increasing number of cancers known to express meiotic proteins.

[2]Co-corresponding authors: Haitong.hou@cuanschutz.edu; Julia.p.cooper@cuanschutz.edu.
[*]Co-first authors

Centromeres and telomeres are widely considered to be independently functioning entities, each essential for accurate chromosome inheritance. Telomeres ensure that chromosome ends are neither fused nor extensively degraded, while centromeres orchestrate the accurate distribution of replicated sister chromatids to daughter cells by attaching to spindle microtubules. We uncovered an instance in which centromere identity depends on telomeres: meiotic centromeres and kinetochores (KT) have a tendency to disassemble, but their reassembly is guaranteed by transient proximity to telomeres[1]. Why centromeres become dismantled during meiosis, and whether this process can occur during proliferative cell divisions, are crucial questions.

The centromere-specific histone H3 variant CenpA underpins assembly and heritability of the multiprotein KT [2,3]. Human centromeres usually assemble over arrays of α-satellite repeats, but these are neither strictly necessary nor sufficient for centromere inheritance. Instead, CenpA is the epigenetic mark that directs this inheritance. CenpA chromatin is generally flanked by heterochromatin (HC) harboring methylated histone H3-lys9 (H3K9me) bound to HP1 proteins[2,4,5]. Canonical *S. pombe* centromeres comprise a unique central core domain of 7–10 kb that harbors Cnp1^{CenpA}, flanked by pericentric HC domains of 40–120 kb. While pericentromeric HC is necessary for CenpA establishment over naïve centromeric sequences, it is dispensable for centromere inheritance[6].

Telomere specification is comparatively straightforward. Chromosome termini comprise simple G-rich telomeric repeats terminating in a 3' single strand overhang, bound by proteins that fulfill the chromosome end-protection functions needed for genome stability[7,8]. Like pericentric regions, telomeres are associated with HC[5,9].

To achieve homologous recombination (HR) and reductional nuclear division, meiotic prophase and meiosis I (MI) encompass key differences from the analogous mitotic phases[10]. During meiotic prophase, HR is initiated by the programmed induction of DNA double strand breaks (DSBs) *via* the meiosis-specific endonuclease Spo11[11,12]; HR repair of those DSBs requires chromosome movements that result in homolog alignment[13]. Meiosis also requires changes in centromeric cohesin patterns[14,15]. While cohesins bind pericentric regions and are largely missing from centromeric cores during proliferative growth, the meiotic Rec8 cohesin complex associates with both regions. Centromeric Rec8 is crucial for monopolar orientation and reductional segregation at MI[16].

A striking and conserved feature of meiosis is the bouquet, the clustering of telomeres at the nuclear envelope (NE)[17–20]. The fission yeast bouquet represents an inversion of mitotic chromosome organization; during mitotic interphase, centromeres cluster at the NE beneath the centrosome (called the spindle pole body, SPB), while telomeres form 2–3 clusters at distal NE regions. In meiotic prophase, telomeres gather beneath the SPB while centromeres disperse; indeed, upon meiotic induction, telomeres cluster gradually before centromeres are released, allowing rare contact between telomeres and centromeres[21].

We reported an unforeseen role for the telomere bouquet in promoting meiotic centromere maintenance[1], finding that centromeres have a small but significant tendency to lose Cnp1^{CenpA} and KTs during meiotic prophase; this is counterbalanced by transient co-

localization of centromeres with the bouquet, which provides a microenvironment that promotes KT reassembly. Hence, at MI and MII, bouquet-defective cells display unattached chromosomes lacking not only KT proteins, but also pericentric HC, indicating a chromatin disruption spanning tens of kilobases. Here we show that the meiosis-defining proteins Spo11 and Rec8 are responsible for this centromere disruption, and that ectopic expression of either in proliferating cells is sufficient to trigger KT loss. These phenomena can be recapitulated in human cells and are likely relevant to cancers that inappropriately express meiotic genes.

Spo11 and Rec8 cause meiotic KT loss

The apparent stability of meiotic centromeres masks a process of occasional centromere dismantlement and reassembly, the latter promoted by localization to the telomere-proximal microdomain[1]. This meiotic centromere reassembly depends on HC, and therefore on the Clr4 histone H3K9 methyltransferase and Swi6[HP1]. Thus, the KT loss phenotype of bouquet-defective (e.g. *bqt1*) cells is phenocopied by *clr4+* or *swi6[HP1]+* deletion. We identified genes whose deletion suppresses the KT loss seen in *bqt1* , *clr4* or *swi6[HP1]* cells. To assess KT loss, we filmed live meiosis in cells harboring endogenously GFP-tagged inner- (Cnp3[CenpC]) or outer- (Ndc80) KT proteins; chromatin, α-tubulin and the SPB were also monitored (Fig. 1a). The 'KT loss' phenotype refers to chromosomes that fail to attach to the spindle at MI or MII and lack KTs; lagging chromosomes with KTs do not fall into this category. While ~2% of *wild-type* (*wt*) cells harboring the four tagged proteins show KT loss, bouquet disruption increases KT loss to ~11% (Fig. 1b–c).

Among a panel of meiosis specific genes (Extended Data Fig. 1a), *rec12[spo11]+* (hereafter referred to as *spo11+*) and *rec8+* emerged as genes whose deletion reverses the KT loss phenotype in *bqt1* , *clr4* and *swi6[HP1]* settings (Fig. 1b–c, Extended Data Fig. 1); hence, Spo11 and Rec8 cause KT loss. The catalytically dead but stable Spo11-Y98F allele (Spo11-cd)[22] failed to suppress KT loss (Fig. 1b, Extended Data Fig. 1b), indicating that KT loss is not a result of DSB formation. In contrast, a point mutation in the Toprim domain that abolishes DNA binding (E179A, Spo11-dbd)[23,24] suppresses KT loss (Fig. 1b, Extended Data Fig. 1b). Deletions of the genes encoding Rec10, Rec11, Rec24, Rec25 or the Spo11 partner TopVIB subunit Rec6, all required for Spo11-mediated DSB induction and recombination[25,26], have no impact on KT loss (Fig. 1b–c, Extended Data Fig. 1a,c), confirming that DNA-bound Spo11 itself, independently of DSB induction, confers centromere dismantlement.

Like Spo11, the meiotic Rec8 cohesin complex is dangerous to centromeres. Rec8 binding to centromeres and chromosome arms requires Psc3 and Rec11, respectively[14]. *rec11+* deletion fails to suppress KT loss (Fig. 1c, Extended Data Fig. 1c) while a *psc3* hypomorph (*psc3–1T*)[27] suppresses KT loss, indicating that centromeric cohesins are specifically responsible.

High Spo11/Rec8 overwhelms KT reassembly

Strong overexpression of Spo11 or Rec8 in a *wt* setting leads to elevated KT loss rates that are increased further by *bqt1+* or *swi6^{HP1}+* deletion (Fig. 1d, Extended Data Fig. 2a–c); weaker overexpression confers KT loss only in the absence of the bouquet (Extended Data Fig. 2a). Overexpression of Spo11-cd, but not Spo11-dbd, causes KT loss at rates rivaling those of *wt* Spo11 (Fig. 1d). *psc3–1T* suppresses KT loss upon Rec8 overexpression (Fig. 1d), confirming that Psc3-dependent centromeric cohesin specifically triggers KT loss. Hence, the ability of the bouquet to promote KT reassembly is insufficient in the face of strongly elevated Spo11 or Rec8.

Budding yeast Rec8 directs Spo11 binding near centromeres[28], suggesting that fission yeast Rec8 promotes KT destruction by promoting Spo11 binding. Perhaps surprisingly, overexpressed Spo11 or Rec8 succeed in elevating KT loss regardless of the respective deletion, *rec8*Δ or *spo11*Δ (Fig. 1d). Moreover, an additive effect is seen when Spo11 and Rec8 are co-overexpressed. Therefore, while at *wt* levels, Spo11 and Rec8 require each other to disrupt KTs in bouquet-defective meiosis, each can disrupt KTs independently when overexpressed.

Chromatin remodelers dismantle KTs

Our observations indicate that Spo11 and Rec8 destabilize or evict CenpA nucleosomes. Moreover, as KT loss also encompasses the loss of H3K9me in pericentric regions[1], such nucleosome destabilization propagates over tens of kilobases to surrounding pericentric HC. We asked whether chromatin remodeling complexes participate in KT loss by deleting genes representing each fission yeast chromatin remodeling complex, CHD, Ino80, Swi/Snf, RSC and Smarcad1. Of these, KT loss is suppressed only by inactivation of CHD or RSC (*via hrp3*Δ and *rsc1*Δ, respectively; Fig. 2A, Extended Data Fig. 2d).

RSC aids cohesin loading during proliferative cell cycles[29,30] by recruiting cohesin loaders and establishing nucleosome free regions. Therefore, the involvement of Rsc1 in KT loss may be exerted *via* meiotic Rec8 loading and clearing of local CenpA nucleosomes. Indeed, *rsc1+* deletion suppresses the ability of Rec8 overexpression to elevate KT loss (Fig. 2b), but has no effect on Spo11 overexpression-mediated KT loss. To determine whether Rsc1 is required for Rec8 loading, we filmed both endogenously tagged (Extended Data Fig. 3) and overexpressed (Extended Data Fig. 4a–b) Rec8-GFP through meiosis. During prophase, Rec8 localizes diffusely throughout the nucleus, reflecting association with numerous chromosomal sites. As cells approach MI, Rec8 disappears along chromosome arms but concentrates near centromeres, forming foci visible in higher brightness images; these foci disappear at MII (Extended Data Fig. 3, 4a–b). When *rsc1+* is deleted, these centromeric foci are vastly diminished, suggesting that Rsc1 promotes KT loss by promoting meiotic centromeric Rec8 loading and local nucleosome displacement.

Hrp3 has been implicated in promoting the regularity of nucleosome spacing downstream of promoters as well as silencing of centromeric and intragenic antisense transcription[31–33]. In contrast to *rsc1+*, *hrp3+* deletion abolishes the KT loss conferred by Spo11 overexpression

(Fig. 2b) while failing to suppress KT loss upon Rec8 overexpression. Hence, Hrp3 may promote Spo11 binding or may be recruited by Spo11 to destabilize local nucleosomes.

Spo11/Rec8 disrupt KTs in mitotic cells

The observation that Spo11 and Rec8 cause meiotic KT loss prompted us to ask whether ectopic expression of these meiosis-specific proteins in proliferative cells would lead to mitotic KT loss. Mitotically expressed Rec8 replaces its mitotic kleisin counterpart, Rad21, and associates with centromeres[14,34]. Western blots confirm that while endogenously myc-tagged Spo11 shows no expression in *wt* mitotic cells, a robust signal is seen when Spo11-myc is ectopically expressed (under *adh1* promoter control); likewise, Rec8 expression is seen only when under *adh1*-control (Fig. 3a). While *wt* cells show occasional lagging chromosomes, these rarely lack KT signal. However, Spo11 expression confers KT loss (Fig. 3b–c). As in meiotic cells, mitotic Spo11-mediated KT loss is reversed upon *hrp3+* deletion; as *hrp3+* deletion has no effect on Spo11 levels (Fig. 3a), we infer that Hrp3 affects Spo11's centromeric activity. Crucially, catalytically dead Spo11 also causes KT loss, while the DNA binding-deficient allele has no effect. Consistently, when a unique centromere, *cen1*, is monitored (*cen1-tetO/R-tomato*), Spo11 expression induces an increase in KT loss corresponding to õne-third of the KT loss rate seen when all three centromeres are monitored (Fig. 3c, Extended Data Fig. 4c–d).

Rec8 expression severely compromises mitotic centromere maintenance, conferring a ~16-fold increase in KT loss (Fig. 3c) or a 5-fold increase at *cen1* (Extended Data Fig. 4c–d). Interestingly, neither mitotic Rec8-mediated KT loss nor mitotic centromeric Rec8-GFP foci are abolished upon *rsc1+* deletion (Fig. 3c, Extended Data Fig. 5a), consistent with previous observations that mitotic cohesin loading can be served redundantly by multiple chromatin remodelers[29,30]. The enhanced KT loss rates seen upon mitotic Spo11 or Rec8 expression are accompanied by a modest increase in the percentage of inviable cells in the population as monitored by staining with methylene blue, which accumulates in dead cells (Extended Data Fig. 5b–c). Hence, Spo11 and Rec8 are each sufficient to disrupt KTs not only during meiotic prophase, but also when ectopically expressed in mitosis.

The *rec8+* transcript contains multiple 'determinant of selective removal' (DSR) sequences, conferring its mitotic Red1-dependent selective removal[35,36], raising the possibility that *rec8+* overexpression saturates this RNA elimination machinery, causing KT loss indirectly *via* overexpression of other DSR genes. However, expression of the DSR genes *crs1+* and *mei4+* is not elevated upon *rec8+* overexpression, while elevation is evident upon *red1+* deletion (Extended Data Fig. 5d), ruling out this indirect effect. Indeed, our observation that *psc3–1T* suppresses the effects of Rec8 overexpression demonstrates that like meiotic Rec8, mitotically expressed Rec8 acts directly at centromeres to cause KT loss (Fig. 3c).

Intriguingly, centromeric enrichment levels in Cnp1[CenpA] chromatin immunoprecipitations (ChIPs) are reduced upon Spo11 or Rec8 expression (Fig. 4a–b, Extended Data Fig. 6a–b). The magnitude of these reductions was initially surprising given that KT loss rates are relatively low (5% and 15%, respectively) in these cells, and suggests that while mitotic Spo11 and Rec8 expression cause a mild overall reduction in centromeric Cnp1[CenpA], only

at a small subset of centromeres does Cnp1^{CenpA} reach below a threshold level that triggers severe KT loss in *cis*. To further evaluate the apparent overall reduction in centromeric Cnp1^{CenpA}, we quantified Cnp1^{CenpA} intensity in single cells whose centromeres remain functional upon Spo11 or Rec8 expression. Remarkably, CenpA intensity is reduced significantly in these cells (Extended Data Fig. 6c), consonant with our ChIP data. Similar reductions were observed when quantifying the outer KT component Ndc80 (Extended Data Fig. 6d), suggesting that the CenpA reduction correlates with a modest reduction in all KT components.

In contrast with CenpA levels, HC levels are slightly increased at the centromeric central core upon Spo11 or Rec8 expression, as evinced by H3K9me2 ChIP (Fig. 4a,c); likewise, the intensities of Swi6^{HP1} foci at centromeres of properly segregating chromosomes increase upon Spo11 or Rec8 expression (Extended Data Fig. 6e). These HC increases are likely due to the mild reduction of centromeric CenpA, as HC spreads into the centromeric core when CenpA levels are compromised[37]. Remarkably, despite the slight increase in pericentric Swi6^{HP1} on segregating chromosomes, Swi6^{HP1} foci are severely reduced or absent from *cen1-tetO/R-tomato* foci on mis-segregating chromosomes upon Rec8 expression (Extended Data Fig. 7a–b). This loss of pericentric HC mirrors the HC loss seen on bouquet-deficient meiotic chromosomes experiencing KT loss[1]. Overexpression of Rec8 in meiosis also triggers loss of Swi6^{HP1} on those chromosomes that fail to segregate (Extended Data Fig. 7c). As each chromosome harbors roughly the same centromere core length but widely varying pericentric HC lengths, our finding that each chromosome has the same KT loss probability[1] suggests that it originates within the CenpA-containing central core. Collectively, our data suggest that modest KT reductions occur at all centromeres upon Spo11 or Rec8 expression but fail to affect KT function and pericentric HC; however, at a subset of centromeres, the balance of CenpA stability *versus* Spo11/Rec8-mediated destabilization is tipped towards catastrophic CenpA reduction, which propagates outward, erasing pericentric HC.

Spo11 or Rec8 expression in human cells confers KT loss

While Spo11 and Rec8 are confined to meiotic cells in mammals as in *S. pombe*, they are inappropriately expressed in specific cancer cell types including melanoma and lung[38,39]. Indeed, meiotic processes are crucial for some cancer proliferation strategies including telomerase-negative ALT telomere maintenance, which requires the meiotic proteins Hop2 and Mnd1 to promote telomere mobility and homology search[40]. Hence, our finding that meiosis-specific proteins spur centromere dismantlement raises the vital question of whether mis-expression of meiotic proteins can lead to centromere dismantlement in human cells. To address this, we constructed stable U2OS cell lines harboring various human Spo11 alleles or Rec8 under control of the inducible Tet-On 3G system[41] (Extended Data Fig. 8a). As for *S. pombe*, three Spo11 alleles were tested: *wt*, catalytically dead (YY137,138FF, Spo11-cd)[42], and an allele harboring a mutation in the putative DNA binding pocket (G251E; Spo11-dbd)[43]. Each cell line was induced for ~48 hours before assessing KT loss. Robust inducible expression was confirmed by fluorescence microscopy and western analyses (Extended Data Fig. 8b–e).

To probe whether human Spo11 and Rec8 confer increased KT loss, we first assessed whether these expressed proteins trigger mitotic defects (Fig. 5a–b, Extended Data Fig. 9a). Indeed, expression of Spo11 (wt and cd, but not dbd) or Rec8 exacerbates the frequency of mitoses with lagging chromosomes or micronuclei, both of which are expected outcomes of KT loss. In contrast, chromosome bridges spanning the two separating nuclei, known outcomes of the constant telomere recombination that occurs in U2OS cells, do not increase upon Spo11/Rec8 expression. Such chromosome bridges cannot stem from KT errors as functional centromeres are required for their formation. Hence, while expressed Spo11, Spo11-cd or Rec8 fail to affect a phenotype that reports on aberrant telomere associations, they confer increased lagging chromosomes and micronuclei.

The mitotic errors conferred by human Spo11/Rec8 expression may evince that these proteins confer KT loss. As very small increases in KT loss are expected to cause substantially increased mitotic error rates (i.e. even one missegregating chromosome could lead to a lagging chromosome or micronucleus), we sought to quantify KT loss in a large number of chromosomes. To visualize KT loss, we monitored CenpA along with CenpB, an inner KT protein that directly binds 'CenpB-box'[44] DNA motifs. CenpB remains at dysfunctional centromeres depleted of CenpA despite loss of other KT proteins[45,46]. Hence, KT loss can be scored *via* the appearance of CenpB chromatin lacking CenpA. CenpB localizes beneath kinetochores[47], displaying a bar-shaped pattern on metaphase chromosomes, with CenpA foci at either end (Fig. 5c, example 1). We developed an algorithm that scores the presence of CenpA staining at either end of each CenpB signal (see Methods; Fig. 5c, Extended Data Fig. 9b–c). A background level of KT loss is seen in the absence of expressed Spo11 or Rec8, likely due to the inherent genomic instability of the multiploid U2OS line[48,49]. However, expression of Spo11 (wt and cd, but not dbd) or Rec8 triggers a significant increase in the number of CenpB bars lacking CenpA (Fig. 5c–d), evincing an increase in KT loss that can readily explain the increase in lagging chromosomes and micronuclei elicited by Spo11 and Rec8. KT loss can occur at one or two end(s) of the CenpB signal, suggesting that CenpA eviction can occur either before or after replication. Thus, KT loss is increased by Spo11 or Rec8 expression, and may be a point of diagnostic or therapeutic application in cancer cells expressing these meiotic proteins.

Discussion

Our observation that CenpA and KT maintenance become precarious during meiosis (Extended Data Fig. 10) raises the specter of imminent danger posed by meiotic processes. Indeed, Spo11/Rec8-mediated dismantlement may contribute to the CenpA decline, KT fragmentation and chromosome segregation errors seen in oocytes from female mammals of advanced age[50,51]. Our observations also lend perspective to emerging ideas about centromere maintenance under varying conditions. While CenpA nucleosome turnover rates are exceptionally low in proliferating metazoan cells[52,53], they are continually destabilized during quiescence or meiotic prophase arrest, necessitating continual CenpA deposition for centromere maintenance and return to proliferation[54]. CenpA destabilization in these scenarios is caused at least in part by ongoing transcription of the underlying DNA. In a separate instance of centromere destabilization, the human SENP6 SUMO protease was identified as a KT maintenance factor in whose absence severe diminution of centromere-

bound KT components is seen[55,56]. Indeed, transcription and sumoylation may play roles in Spo11- and Rec8-mediated KT loss.

Mild levels of Spo11- or Rec8-mediated CenpA disruption fail to spread into surrounding HC; however, severe CenpA disruption quashes this opposition, spreading disruption to the pericentric HC (Fig. 4, Extended Data Fig. 6). The mechanisms underlying this transition from mild to catastrophic centromere disruption are under investigation. As pericentric HC is required for *de novo* establishment of CenpA chromatin[6], disruption of pericentric HC triggers loss of local CenpA reassembly potential. Indeed, the role of the telomere bouquet in promoting meiotic KT reassembly stems from the provision of telomeric HC in *trans* (HH, EK and JPC, in preparation).

Whether the potential centromere disruption imposed by Spo11 and Rec8 serves a positive role in meiosis is a crucial question. Assembly of the monopolar attachment machinery could be facilitated by transient dismantlement. Indeed, dissociation of outer KT components promotes monopolar attachment at budding yeast MI[57]. Moreover, centromere dismantlement can be considered risk-free in *wt* meiosis, as colocalization of centromeres and telomeres in early prophase during bouquet formation ensures that centromere reassembly is robust[1] (Extended Data Fig. 10). In contrast, proliferating cells lack the bouquet and have no backup system to ensure centromere reassembly.

Overexpressed KT components are markers of cancers experiencing high levels of genome instability, and therefore heightened sensitivity to DNA damaging agents[58]. Our results suggest an additional mode of cancer cell vulnerability due to insufficient maintenance of centromeres upon Spo11 or Rec8 expression. The increasingly recognized tendency of cancer cells to express meiotic genes[38,39] makes it essential to understand the consequences of this aberrant gene expression. Their meiosis-specificity among non-cancer cells would confer an obvious advantage to anti-cancer strategies targeting vulnerabilities introduced by Spo11 or Rec8.

Methods

Yeast strains and media

Details of strains are listed in Supplementary Table 1. *spo11* mutations were introduced by replacing *ura4* previously inserted at the endogenous *spo11* locus and were verified by sequencing. For overexpression constructs, the open reading frames of *spo11* with and without indicated mutations were cloned into pREP41 or pFA6a plasmids (under *nmt41* or *adh1* promoters, respectively) and then integrated at the *S. pombe nmt1* termination site or *adh1* promoter for overexpression. For lower levels of overexpression, *spo11* was cloned into the pFA6A plasmid under control of the *adh13* promoter, then integrated at the endogenous *spo11* locus. Gene deletions of chromatin remodelers and C-terminal tagging of *Pht1*[H2AZ1] and *Cnp3*[CenpC] were created by PCR-based gene replacement [59]. Other mutants were obtained from the Japanese National Bioresource Project or as described previously [60–62]. Strains with multiple mutated genotypes were generated by mating, sporulation and selection for recombinants. Media were as described (PombeNet; https://dornsife.usc.edu/pombenet/media/).

For overexpression of inducible *nmt41-spo11* in meiotic cells, cells were grown in minimal media lacking thiamine to induce *nmt41* for 24 hours before meiotic induction.

Cell culture and stable cell line generation

U2OS cells (a generous gift from Eros Lazzerini Denchi; originally from ATCC) were grown in DMEM media supplemented with 10% FBS and 1% Penicillin–Streptomycin-Glutamine at 37 °C in a 5% CO_2 incubator. Mycoplasma infection was routinely ruled out. Inducible stable cell lines were generated by transposition with the piggyBac transposase as previously described[63]. Briefly, one day prior to transfection, cells were seeded at a density of $1.25–2.5 \times 10^5$ cells/ml. Plasmids (the piggyBac vector along with the helper plasmid encoding the piggyBac transposase) were transfected with Lipofectamine 3000 (Life Technologies) in a 2:1 ratio according to the manufacturer's instructions. Six hours after transfection, the medium was exchanged with medium containing Tetracycline-free FBS (Hyclone), to avoid leaky expression of the piggyBac vectors. Two days post transfection, cells were selected with Hygromycin B (250 μg/ml) for one week and expanded for downstream analysis. Cell lines were kept in Tetracycline-free medium containing Hygromycin B (250 μg/ml).

Spo11-myc-DDK from an Origene plasmid (NM_012444) was cloned into a pEGFP-N1 vector (a kind gift from Dr. Paul Meltzer). Mutations of Spo11 were introduced *via* overlapping PCR followed by replacement cloning of the original Spo11 into pEGFP-N1; mutations were confirmed by sequencing. Spo11 encoded in these constructs was amplified by PCR and introduced to a vector containing the Tet-ON 3G-inducible promoter (TREG), GFP and recognition sites for piggyBac transposase (piggyBac vector) (a kind gift from Dr. Iain Cheeseman) by Gibson assembly. Rec8 from an Origene plasmid (NM_005132) was introduced by Gibson assembly to the piggyBac vector.

Microscopy

Microscopy images were captured on a DeltaVision microscope system (GE Healthcare Life Sciences) equipped with an Olympus IX70 widefield inverted epifluorescence microscope, an Olympus UPlanSapo 60x NA 1.42 oil immersion objective, and a Photometrics CCD CoolSnap HQ camera. For each experiment, images were acquired with identical settings of light intensity, exposure time, number of focal planes and step size. Images were deconvolved and projected into a 2D image with the maximum intensity projection setting by SoftWorx (GE Healthcare Life Sciences). Image processing and analysis were performed using SoftWorx and ImageJ-based software Fiji.

For live cell imaging of meiosis, h^{90} or a mixture of h^+ and h^- cells grown to log phase at 30°C on EMM plates with required supplements were spotted on SPA plates at 30°C for 5–7 hours before live microscopy. Cells were adhered to 35 mm glass culture dishes (MatTek) with 0.2 mg/ml soybean lectin (Sigma) and immersed in 3 ml EMM lacking a nitrogen source with required supplements. Time-lapse images were acquired at 30°C in an Environmental Chamber with a DeltaVision Spectris (GE Healthcare Life Sciences) at intervals of 15 minutes. For cells containing Sid4-mCherry, mCherry-Atb2, Pht1^{H2AZ}-mCherry and either Cnp3^{CenpC}-GFP or Ndc80–2xGFP, images were acquired

over 22 focal planes with a 0.4 μm step size at intervals of 15 minutes. A meiotic KT loss event was scored if at least one chromatin mass of Pht1[H2AZ]-mCherry remained unsegregated and lacked detectable KT signal. For cells containing Sid4-mCherry, mCherry-Atb2 and Rec8-GFP, images were acquired over 22 focal planes with a 0.4 μm step size at intervals of 10 minutes. For cells whose *centromere 1* was visualized with *tetO/R-tomato* on *dh1L(cen1)::tetO* (*cen1-tetO/R-tomato*), images were acquired at 15 focal planes with a 0.6 μm step size. A meiotic event was scored if a centromere 1 remained unsegregated and lacked detectable Swi6[HP1]-GFP signal.

To examine live mitosis in cells containing *cen1-tetO/R-tomato*, cells grown in YES media at 32°C to mid-log phase were adhered to 35 mm glass culture dishes (MatTek) with 0.2 mg/ml soybean lectin (Sigma) and immersed in 3 ml YES (for cells containing Ndc80–2xGFP) or EMM with required supplements (for cells containing Swi6[HP1]-GFP). Images were acquired at 15 focal planes with a 0.6 μm step size. Cells were designated as late anaphase if the distance between spindle poles was greater than 6 μm; these were analyzed for lagging chromosomes. A lagging *centromere 1* was scored as lacking KT or HC, respectively, if the lagging chromosome harbored *cen1-tetO/R-GFP* but no detectable Ndc80–2xGFP or HP1[Swi6]-GFP signal.

To examine mitosis in ethanol-fixed samples, cells were grown to mid-log phase (OD_{595nm} = 0.5) in YES media at 32°C and kept in the dark on ice throughout the procedure until imaging. Cells were centrifuged at 3,000 rpm for 2 minutes, resuspended in 1ml 70% ethanol on ice, and incubated for 15 minutes; subsequent steps were also performed on ice. Fixed cells were centrifuged at 3,000 rpm for 30 seconds and resuspended in 1 ml water for rehydration, then centrifuged, resuspended in 1ml PBS containing 5 μg DAPI, and incubated for 3 minutes followed by three washes with 1 ml PBS. Images (size = 2048×2048 pixels) were acquired at 25 focal planes with a 0.4 μm step size; an identical exposure sequence of mCherry/FITC/DAPI was used for all images. Deconvolved images were projected as 2D images with the maximal intensity setting and analyzed with Fiji. Cells were designated as late anaphase when the distance between two SPBs (Sid4-mCherry dots) was greater than 6 μm; these were subjected to analysis for lagging chromosomes. To measure the intensities of centromeric proteins on properly segregating chromosomes, cells lacking lagging chromosomes were selected. For any analyzed fields, all qualified cells were measured to avoid bias. The mean intensity within a circle (diameter = 0.76 μm) including the Cnp1[CenpA]-GFP, Ndc80–2xGFP or Swi6[HP1]-GFP focus was measured, background subtracted and divided by background. The background was assigned as the mean intensity of two nearby circles with identical 0.76 μm diameter within the same cell.

To examine GFP expression and chromosome mis-segregation in interphase and mitotic U2OS cells, respectively, the cells were plated onto glass coverslips and induced by addition of doxycycline (1 μg/ml). Two days later (~48–50 hours), cells were fixed in 4% paraformaldehyde/PBST (1XPBS/0.1% Triton X-100). To investigate kinetochore loss, metaphase spreads were prepared as previously described[64]. Briefly, following mitotic shake off, cells were blocked in metaphase with 1μg/ml Colcemid and incubated at 37°C for 30 minutes. The supernatant was collected and mixed with adherent cells after their trypsinization. The cells were pelleted by centrifugation and were counted. For each slide,

1.5×10^5 cells were resuspended in 75mM KCl, incubated at room temperature (RT) for 10 minutes and cytospun onto a glass slide in a single-chamber funnel for 10 minutes at 900 rpm on high acceleration, in a Shandon Cytospin 4. Cells were fixed as described above.

For immunofluorescence, cells were washed once in PBST and blocked in 1% BSA/PBST at RT for at least 30 minutes. Primary antibodies (CenpA (Abcam ab13939), CenpB (Abcam ab25734)) were incubated overnight at 4 °C. Secondary antibodies coupled to Alexa Fluor 555 and 647 (Invitrogen) were incubated for one hour at RT. All antibodies were used at 1:100 dilution, in 1% BSA in PBST. DNA was counterstained with DAPI in PBST (5 μg/ml), and coverslips were mounted on slides with Vectashield (Vector Laboratories). All images were taken as 50 Z-stacks of 0.2 μm increments, using the same exposure conditions for each genotype processed in a given experiment. Images were deconvolved on a SoftWorx Explorer Suite (Applied Precision) and analyzed on Fiji as described below.

To assess chromosome segregation defects, the presence of DAPI signal disconnected from the dividing nuclei was assessed blindly. Projections of maximum intensity are shown. Statistical analysis was performed with Prism 8 (GraphPad Software), using Fisher's exact tests.

Semi-automated quantitation of KT loss

We developed a Fiji/ImageJ macro to score for the presence of CenpA signal on either side of a CenpB bar. For each imaged field of chromosome spreads (karyotype), we selected non-overlapping centromere pairs for analysis, as well as a number of equivalent-sized areas for background subtraction. This was the only manual step in the method, and was performed blind by initially viewing only the channels representing CenpB and DAPI.

The rest of the automated method proceeded as follows. To improve signal-to-noise, each image was denoised by 2D anisotropic diffusion, subjected to background (average intensity of selected background regions) subtraction, and normalized (pixel intensities were divided by average background, then by the mean of all selected centromere regions). Individual centromere pairs were oriented horizontally along the length of the CenpB bar, and the CenpA/B intensity profiles along this horizontal axis were computed. A peak counting method determined the number of CenpA peaks (maxima) above background in the intensity profiles. As appropriate, a single Gaussian or linear mixture of two Gaussians was fit to the CenpA/B intensity profiles. The output was the number of CenpB half-bars (centromeres) lacking CenpA, after discarding bad fits ($r^2 < 0.75$) and completely overlapping CenpA/B profiles.

We aggregated the output from multiple images for each group (genotype ± doxycycline) from three independent experiments and calculated the percentage of centromeres lacking CenpA. We used GraphPad Prism 9 to perform two-sided Fisher's exact tests for statistical significance and to compute 95% confidence intervals for the odds ratios, comparing induced vs uninduced samples for each genotype.

Bootstrapping

To examine, in a statistically rigorous manner, the validity of pooling data from multiple experiments quantifying KT loss, we used bootstrapping to assess the possible spread of experimental outcomes for each group (genotype ± doxycycline). Briefly, given a set of data points containing the number of CenpB half-bars (centromeres) lacking CenpA per karyotype from three independent experiments for a particular group, we used GNU Octave 4.4.1 to randomly resample with replacement from this set 100 times. For each iteration, we computed the percentage of centromeres lacking CenpA. Using these 100 estimates per group, we plotted the mean ± standard deviation (SD) of the percentage of centromeres lacking CenpA using GraphPad Prism 9 (Extended Data Fig. 9c). The bootstrapped estimates provided sufficient statistical power to perform tests that take into account variation both within and between groups; we performed an ordinary one-way ANOVA (assuming equal SDs) and Sidak's multiple comparison test (comparing the means of induced vs uninduced samples for each genotype). We determined that there was low variation within groups, and thus between samples of the same genotype from different experiments, justifying the pooling of data from multiple experiments; we also found a statistically significant difference in the mean estimate of percentage of centromeres lacking CenpA upon doxycycline induction for each genotype.

Methylene blue staining

20ml of *S. pombe* cells grown to mid-log phase in YES media at 32°C were centrifuged at 3,000 rpm for 2 minutes and washed twice with 1 ml PBS (pH 7.4) at room temperature. Cell pellets were resuspended in 100 μl PBS, mixed with 100 μl 0.0002% methylene blue in PBS, and incubated in the dark at room temperature for 5 minutes. Cells were then centrifuged, washed twice in 1 ml PBS and kept in the dark before imaging. Snapshots of methylene blue-stained cells were acquired at the setting for Cy5 (excitation at 632 nm and emission at 679 nm) and overlaid on brightfield images for scoring.

ChIP analysis

ChIP experiments were performed as described with the exception of the final purification step [65]. In brief, cells grown in EMM with required supplements (for experiments with Spo11.OE1 cells) or YES (for experiments with Rec8.OE cells) to mid-log phase were cross-linked with 3% paraformaldehyde and vigorously shaken with glass beads for lysis. The lysates were cleared by centrifugation, sonicated to generate DNA fragments with sizes of 0.5–1 kb, and immunoprecipitated with anti-Flag antibodies conjugated to magnetic beads (Sigma-Aldrich; for each reaction, 15 μl), anti-GFP antibodies (Abcam ab290, 3 μg/ml lysate) or anti-H3K9me2 antibodies (Abcam 1220, 3 μg/ml lysate); the latter two were subjected to pull-down with Protein G dynabeads (Thermo Fisher; 15 μl). The crosslinking was reversed, and DNA was purified with the Qiaquick PCR purification kit. Quantitative real-time PCR was performed with SYBR green master mix (Roche) in a real-time PCR system (Applied Biosystems), and data were analyzed with Microsoft Excel (Microsoft, version 16.29.1). For each primer pair, serial dilutions of DNA were used as templates to generate a standard curve of amplification for each plate of PCR reactions, and the relative concentration of target sequence was calculated accordingly. The enrichment of a

target sequence in immunoprecipitated DNA over whole-cell extract was calculated and normalized to that of a reference sequence (*act1*).

Primers used for ChIP analysis:

act1: GATTCTCATGGAGCGTGGTT / GGAGGAAGATTGAGCAGCAG

centromere core: AAAAGGCCGGCTCATTTATAG / AGGCGATTGAAATCCCTTTA

Analysis of Gene Transcription

Total RNA was extracted from *S.pombe* cells at mid-log phase using the MasterPure™ Yeast RNA Purification Kit (Epicentre). Reverse transcription and real-time quantitative PCR were performed with a mixture of SuperScript™ III Reverse Transcriptase (Invitrogen) and SYBR green master mix (Roche). Serial dilutions of RNA were used as templates to generate the standard curve for each target sequence. The relative concentration of target sequence in each sample was calculated accordingly and normalized to that of a reference sequence (*act1*). For each gene, the RNA level in wild type cells served as a reference for normalization.

Primers used for transcription analysis

act1: GATTCTCATGGAGCGTGGTT / GGAGGAAGATTGAGCAGCAG

crs1: TGCGCTTCGTTCTGGGTCTT / TCTGCAGAACCATTTGTGGGCA

mei4: ACCGTTGACGACGCGAGAGA / GCATCGTTTGAGACTTCGGCAGC

Western Blotting

25 OD_{595} units of *S. pombe* cells (approximately $3.7–5 \times 10^8$ cells) at mid-log phase were vigorously shaken with glass beads. 300 µl lysates in Laemmli buffer were heated at 95°C for 5 minutes and cleared by centrifugation. The supernatant was diluted 8-fold in Laemmli buffer, and 10–15 µl of each sample used for SDS-PAGE and western transfer. Expression of myc-tagged Spo11 and HA-tagged Rec8 was detected with antibodies against Myc (BioXcell at 1:50,000 dilution) and HA (Abcam ab9110 at 1:5,000 dilution). Cdc2 was detected with antibody from Santa Cruz Biotechnology (Sc-53 at 1:5,000 dilution) and served as loading control.

For western blot analysis of U2OS cell lines, extracts were prepared as previously described[64]. Following trypsinization, cells were resuspended in 2X Tris–Glycine SDS sample buffer (Novex, Life Technologies) at a concentration of 2.5×10^4 cells/µl, sonicated for 5 cycles of 30s (high) and boiled for 5 min at 95 °C. GFP expression was detected with an antibody against GFP (Abcam ab290 at 1:5,000 dilution). Endogenous Spo11 expression was detected with a rabbit monoclonal (clone MB36–4) antibody against Spo11-β isoform (generous gift from Dr. D. Camerini-Otero[66]) at 1:500 dilution. As a loading control tubulin was detected (Abcam ab6160 at 1:5,000 dilution) on the same blots.

Software availability

The Fiji/ImageJ macro to score for the presence of CenpA signal on either side of a CenpB bar is available (Supplementary Software) under a GNU General Public License v3.0, and has been tested on Fiji/ImageJ 2.0.0-rc-69/1.53b.

Data Availability

Source data are provided with this paper. Reagents and any further information are available on request to JPC or HH.
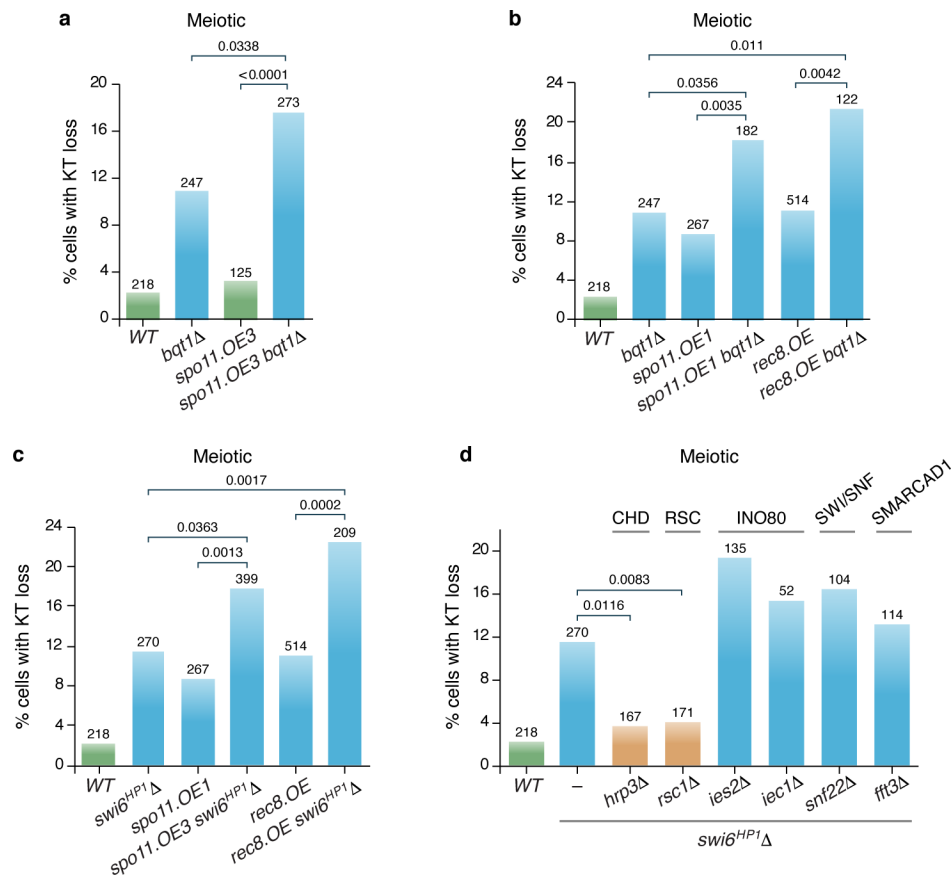
Extended Data
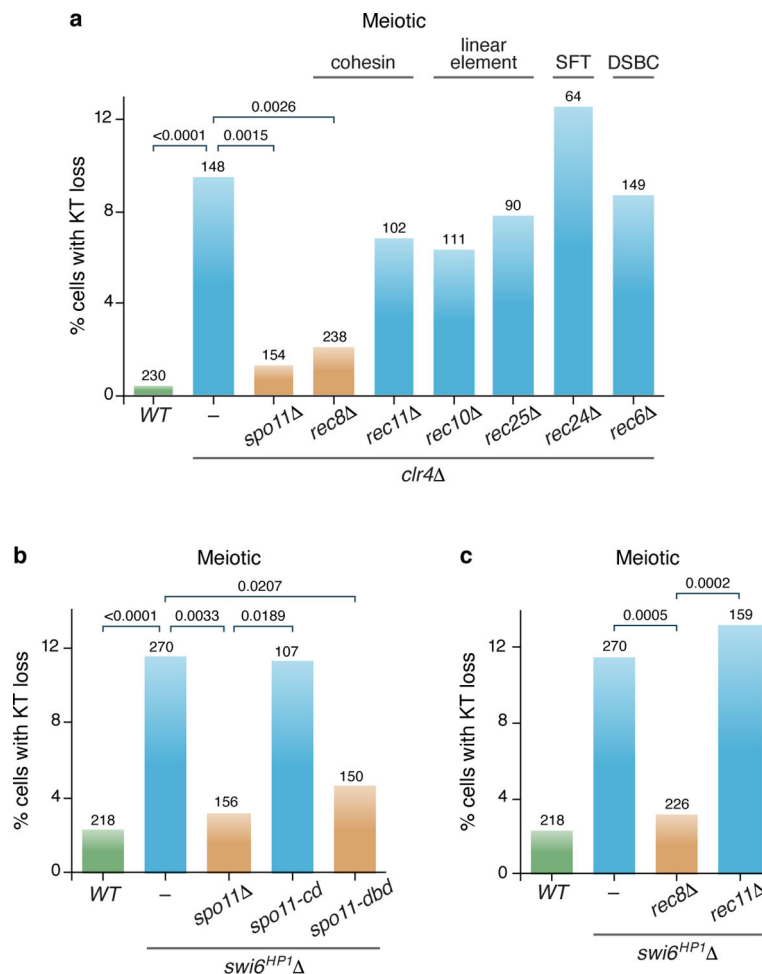
**Extended Data Fig. 1. Spo11 and Rec8 cause meiotic KT loss in the absence of HC.**
Quantitation of KT loss phenotypes as exemplified in Figure 1a. KTs are visualized with Ndc80–2xGFP (a) or Cnp3^{CenpC}–GFP (b-c). (a) *spo11Δ* and *rec8Δ* rescue KT loss in *clr4Δ* cells while deletions in other subcomplexes[25] of the meiotic recombination machinery do not. (b) *spo11+* deletion or the DNA binding-deficient *spo11-dbn* mutant rescue KT loss in the absence of Swi6^{HP1}, while *spo11-cd* triggers KT loss as does *wt spo11*. (c) *rec8+* deletion, but not *rec11+* deletion, suppresses KT loss in the absence of Swi6^{HP1}, mirroring

these proteins' effects in *bqt1* cells. Total numbers of films analyzed are indicated above each bar. p values are determined by two-tailed Fisher's exact tests and indicated above brackets.

Extended Data Fig. 2. Overexpression of Spo11/Rec8 elevates KT loss rate, and chromatin remodelers are required for meiotic KT dismantlement.
Quantitation of KT loss phenotypes as in Figure 1a. (a) Expressing a tandem copy of *spo11+* under the control of weaker (relative to *adh1* or *nmt41*) *adh13* promoter (*spo11.OE3*) does not confer KT loss in a *bqt1+* setting, but increases KT loss in the *bqt1* setting. (b-c) Strong overexpression of *spo11+* (*spo11.OE1,* controlled by *nmt41* promoter) or *rec8+* (*rec8.OE,* controlled by *adh1* promoter) elevates the frequency of meiotic KT loss in *bqt1* (b) and *swi6* (c) settings. Total numbers of films analyzed indicated above each bar. p values are determined by two-tailed Fisher's exact tests and indicated above brackets. (d) Loss of a CHD remodeler (Hrp3) or RSC component (Rsc1) rescues KT loss in the absence of *swi6^HP1^*; other chromatin remodelers have no effect. Total numbers of films analyzed indicated above each bar. p values are determined by two-tailed Fisher's exact tests and indicated above brackets.
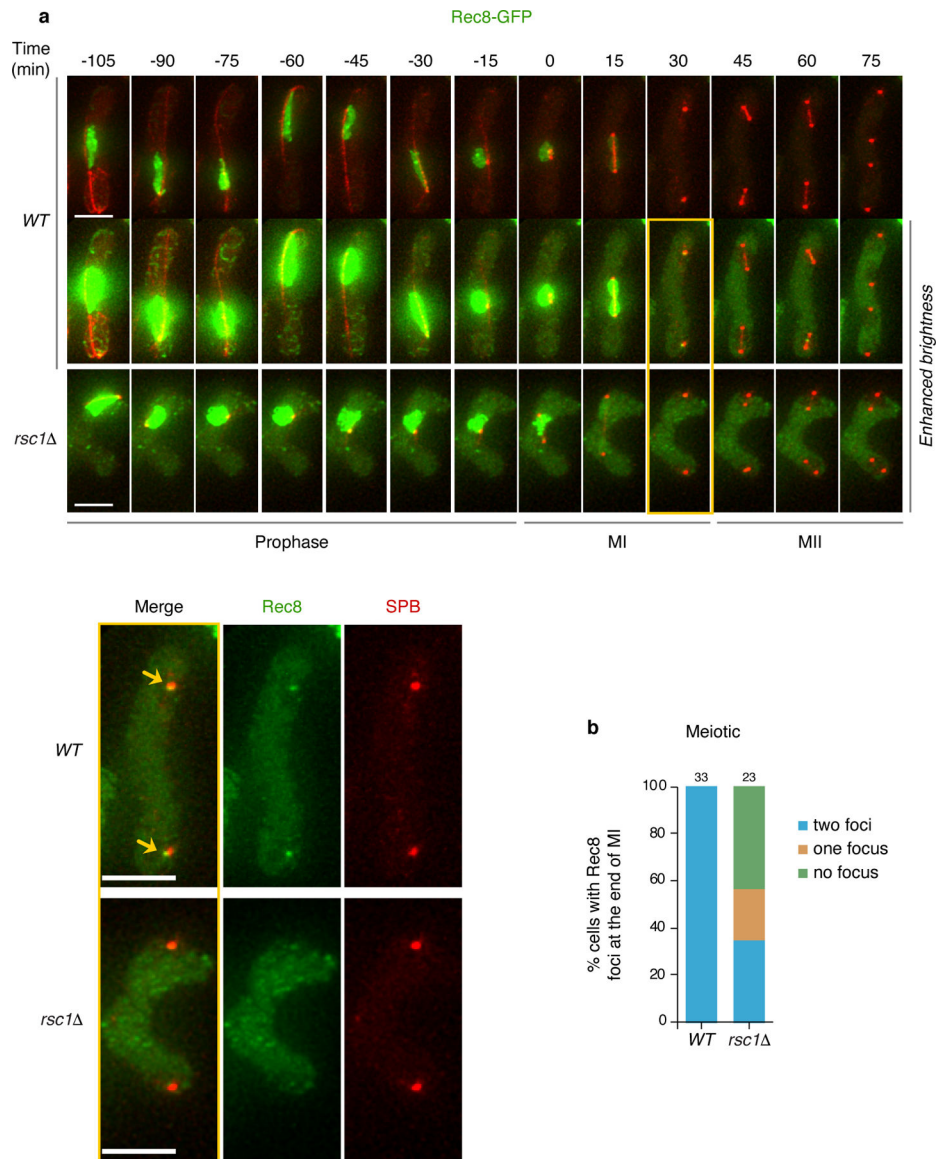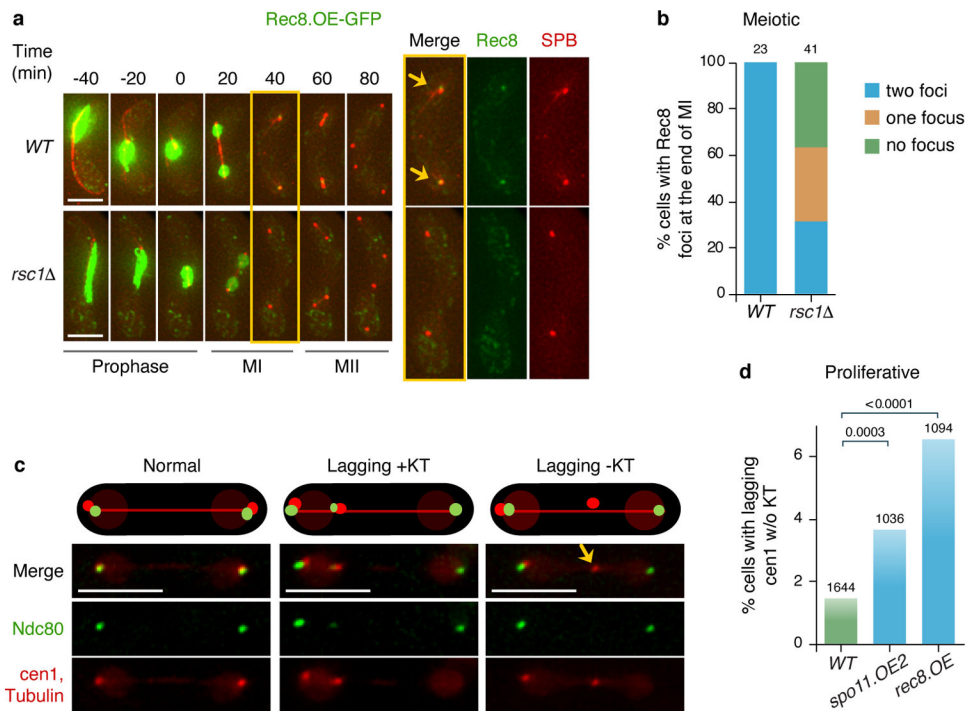
Extended Data Fig. 3. RSC facilitates Rec8 localization to meiotic centromeres.
(a) Frames of representative films monitoring endogenously GFP-tagged Rec8 through meiosis are shown. During prophase, Rec8 localizes throughout the nucleus. As cells approach MI, Rec8 begins to disappear but remains concentrated at centromeres, as seen at enhanced brightness. At the end of MI, Rec8 foci are clearly visible in the *wt* cell but not in the *rsc1* cell. The frames highlighted in the yellow box are shown below; these foci subsequently disappear at MII. Scale bars = 5μm.
(b) Quantitation of meiotic cells harboring zero, one or two Rec8 foci at the end of MI. Total numbers of films analyzed are indicated above each bar. All *rsc1* films show diminished Rec8-GFP at the end of MI, and most of them fail to show any detectable Rec8-GFP on at least one SPB.

Extended Data Fig. 4. RSC facilitates overexpressed Rec8 localization to meiotic centromeres, and expression of Spo11 and Rec8 in proliferating cells causes KT loss as visualized *via* a fluorescent array on *cen1*.

(a) Frames of representative films monitoring overexpressed Rec8-GFP through meiosis. During prophase, Rec8 localizes throughout the nucleus. As cells approach MI, Rec8 begins to disappear but remains concentrated at centromeres. At the end of MI, Rec8 foci are clearly visible in the *wt* cell, but not in *rsc1* cells. The frames highlighted in the yellow box are enlarged in the right-hand panels; these foci subsequently disappear at MII. Scale bars = 5 μm.

(b) Quantitation of meiotic cells harboring Rec8 foci at the end of MI. Total numbers of films analyzed are indicated above each bar. All *rsc1* films show diminished Rec8-GFP at the end of MI, and most fail to show any detectable Rec8-GFP on at least one SPB.

(c) Top: schematic outlining the loss of KT components on *cen1* in anaphase cells. Below: Images of live cells in late anaphase; the KT is visualized with Ndc80–2xGFP, *cen1 via cen1-tetO/R-tomato*, and the spindle *via* mCherry-Atb2. Arrows indicate lagging *cen1* with KT loss. Lagging *cen1* with intact KT is also shown (right-hand panel) but is excluded from quantitation. Scale bars = 5μm. (d) Quantitation of *cen1* KT loss as exemplified in (a). Expression of Spo11 or Rec8 increase the anaphase KT loss of *cen1*. Total numbers of cells analyzed are indicated above each bar. p values are determined by two-tailed Fisher's exact tests and indicated above brackets.
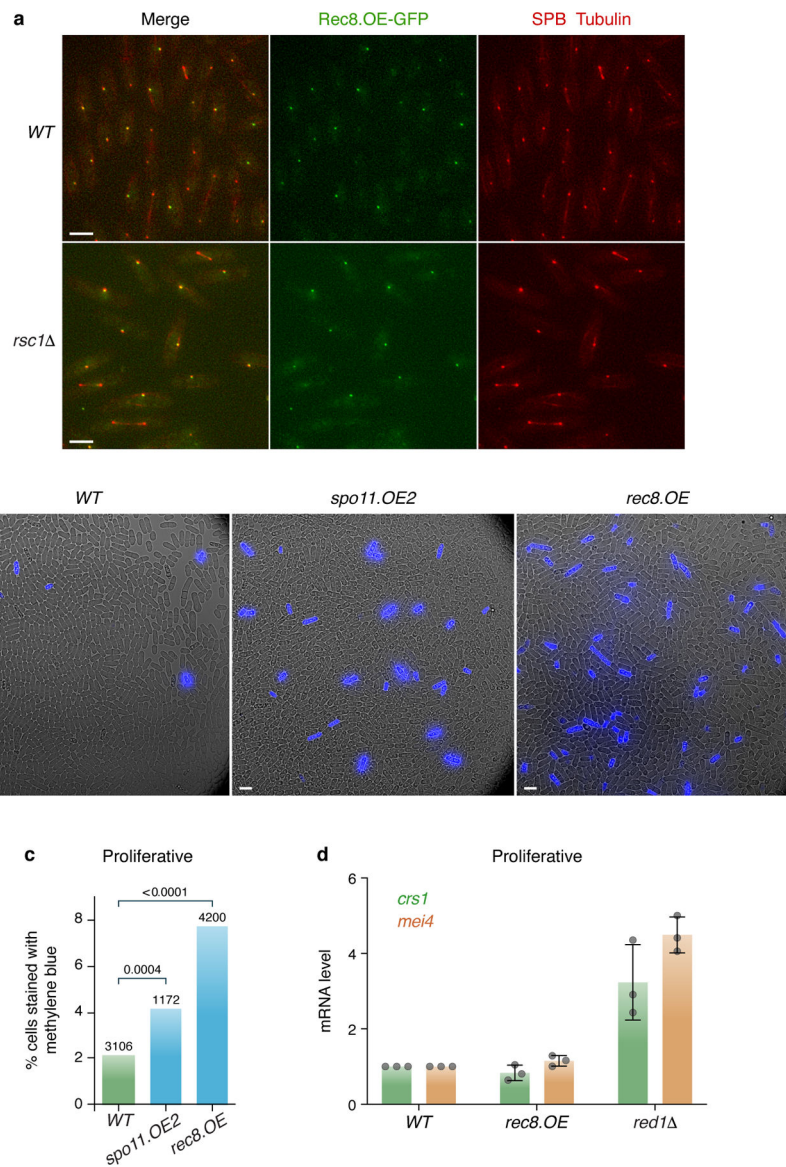
Extended Data Fig. 5. Expression of Spo11 or Rec8 in proliferating cells causes KT loss and cell death, directly and independently of RSC.

(a) Deletion of *rsc1+* does not affect centromeric localization of Rec8 in proliferating cells. Representative images of proliferating cells expression Rec8-GFP based on two independent experiments. Rec8-GFP forms foci at centromeres that co-localize with SPBs. No visible change in the intensity of these Rec8 foci is observed upon *rsc1+* deletion. Scale bar = 5 μm. (b) Expression of Spo11 or Rec8 increases the percentage of inviable cells. Representative images of fields of cells stained with methylene blue, which cannot be exported from inviable cells. Scale bars = 10 μm. Quantitation of 1 representative experiment (of three performed) is shown in (c). (d) Rec8 overexpression does not affect expression of other DSR-containing genes. The levels of *crs1* and *mei4* transcripts are elevated by *red1+* deletion but not affected by *rec8+* overexpression. Total RNA was extracted and analyzed by Real-time PCR with primers annealing to *crs1+* and *mei4+*. The expression level is

normalized against that of *act1+*, and then with that of a control *wt* strain. Mean expression levels and standard deviations are calculated based on 3 repeats of each genotype.
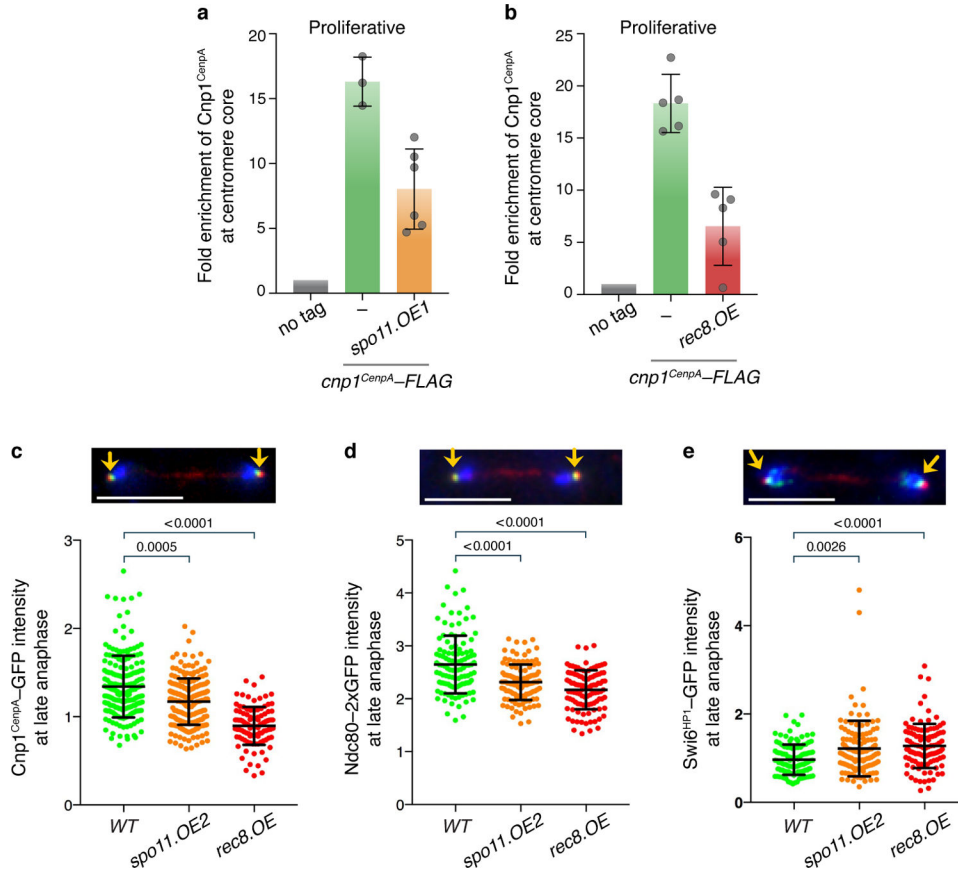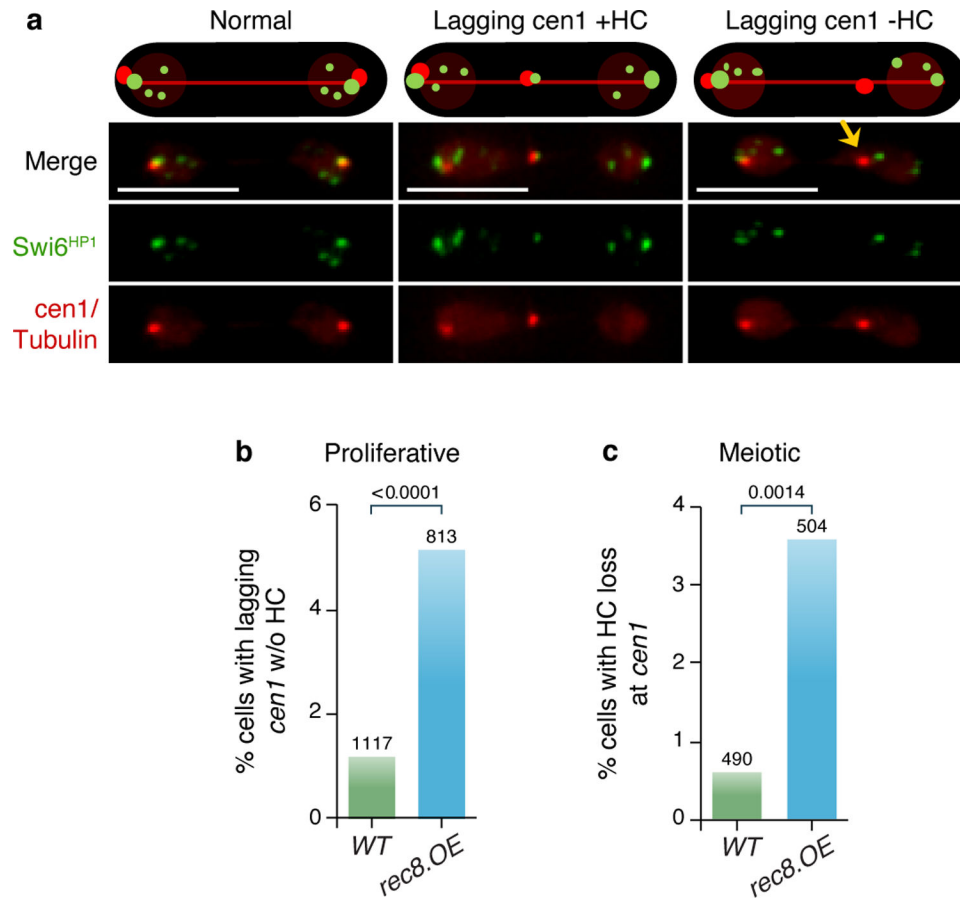

Extended Data Fig. 6. Expression of Spo11 and Rec8 reduces levels of CenpA at functioning KTs.
(a-b) ChIP analysis of Cnp1^{CenpA} at centromeric central core region. Endogenously 3xFlag-tagged Cnp1^{CenpA} was immunoprecipitated with anti-Flag antibody and analyzed by Real-Time qPCR using a primer pair annealing to the central cores of chromosomes I and III. Enrichment level is normalized against that of *act1+*, and then with that of a control *wt* strain with no tag on Cnp1^{CenpA}. Spo11 was expressed under control of *nmt41* (*spo11-OE1*) and cells were grown under conditions that induce *nmt41* (minimal media). Mitotic Cnp1^{CenpA} enrichment at the central core is reduced upon expression of Spo11(a) or Rec8 (b), as is the case for cells overexpressing Spo11 under the *adh1* promoter, or Rec8 under *adh1* control, in rich media (Fig. 4b). The values for each biological replicate are shown as grey dots. Mean enrichment and standard deviations are shown in bars.

(c-e) Expression of Spo11 and Rec8 confers overall reduction of KT components on properly segregating chromosomes. Dotplots of Cnp1^{CenpA}-GFP, Swi6^{HP1}-GFP and Ndc80-GFP intensity on segregated chromosomes (see Methods). Anaphase cells without lagging chromosomes, as exemplified in the images atop each graph, were analyzed, using the same strains as in Figure 4. Arrows indicate foci whose intensities are measured. Each dot in the plot represents a distinct centromere focus. Mean intensity and standard deviation are shown for a representative experiment of two or more performed. Spo11 or Rec8 expression

reduces Cnp1^{CenpA} and Ndc80 intensity (c,e) on properly segregated anaphase centromeres, but modestly increases Swi6^{HP1}-GFP intensity (d). p values are determined by Kolmogorov-Smirnov tests and indicated above brackets. Scale bars = 5 μm.


Extended Data Fig. 7. Expression of Rec8 leads to HC loss on lagging *cen1*.
(a) Top: Schematic of possible *cen1* and *HC* focus behaviors in anaphase cells; HC (represented by Swi6^{HP1}-GFP) localizes to large centromeric foci as well as multiple small subtelomeric foci. Below: Images of live cells in late anaphase; HC is visualized *via* Swi6^{HP1}-GFP, *cen1 via cen1-tetO/R-tomato*, and microtubules *via* mCherry-Atb2. Arrows indicate lagging *cen1* with HC loss. Lagging *cen1* with intact HC is excluded from quantitation. Scale bars = 5 μm.
(b) Quantitation of *cen1* HC loss as exemplified in (A). Expression of Rec8 causes anaphase HC loss at *cen1*. Total numbers of cells are indicated above each bar. p values are determined by two-tailed Fisher's exact tests and indicated above brackets.
(c) Quantitation of HC loss on unsegregated *cen1* during meiosis. Overexpression of Rec8 during meiosis increases the incidence of unsegregated *cen1* lacking detectable Swi6^{HP1}-GFP. Total numbers of films analyzed are indicated above each bar. p values are determined by two-tailed Fisher's exact tests and indicated above brackets.
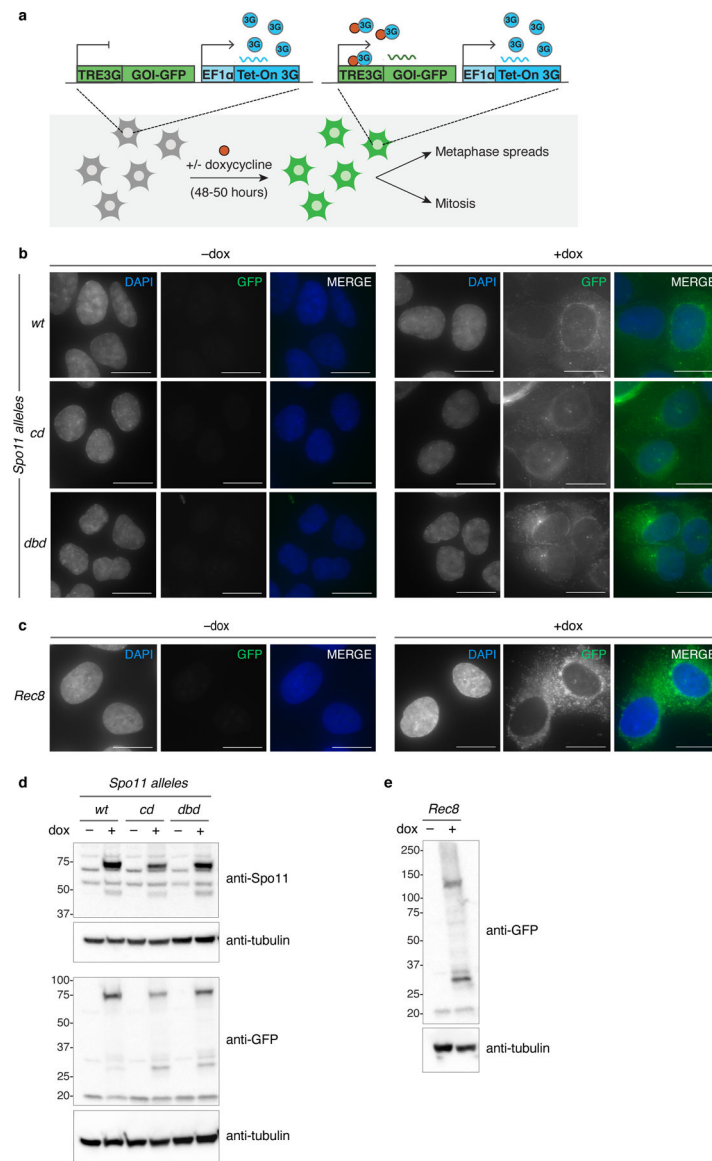
Extended Data Fig. 8. Inducible expression of Spo11 alleles and Rec8 in U2OS cells

(a) Experimental setup for inducible expression of Spo11 alleles and Rec8 in U2OS cells. Schematic of Tet-ON system used for inducible expression of GFP-tagged genes of interest (GOI) (upper panel). The reversible tetracycline activator (Tet-ON 3G) is constitutively expressed under regulation of the EF1α core promoter. Addition of doxycycline (dox) induces binding of the transactivator 3G (blue circles) to the TRE3G promoter, inducing expression of the GOI.

(b,c) Representative images of fixed cells with or without addition of doxycycline. Spo11 (b) and Rec8 (c) are C-terminally tagged with GFP and nuclei are counterstained with DAPI. Scale bars = 20μm. While Spo11/Rec8 localize largely to the cytoplasm, all alleles enter the nucleus as well.

(d) Western blots probed with anti-Spo11 or anti-GFP antibody show no detectable expression of endogenous Spo11 (predicted ~44kDa), but show robust induced expression

of the GFP tagged Spo11 alleles (predicted size ~82.5KDa). Loading is controlled with an antibody against tubulin, and westerns were performed three times with identical results. (e) Western blot probed with anti-GFP antibody shows expression of tagged Rec8 (predicted ~100KDa) upon doxycycline induction. Loading is controlled with anti-tubulin antibody.
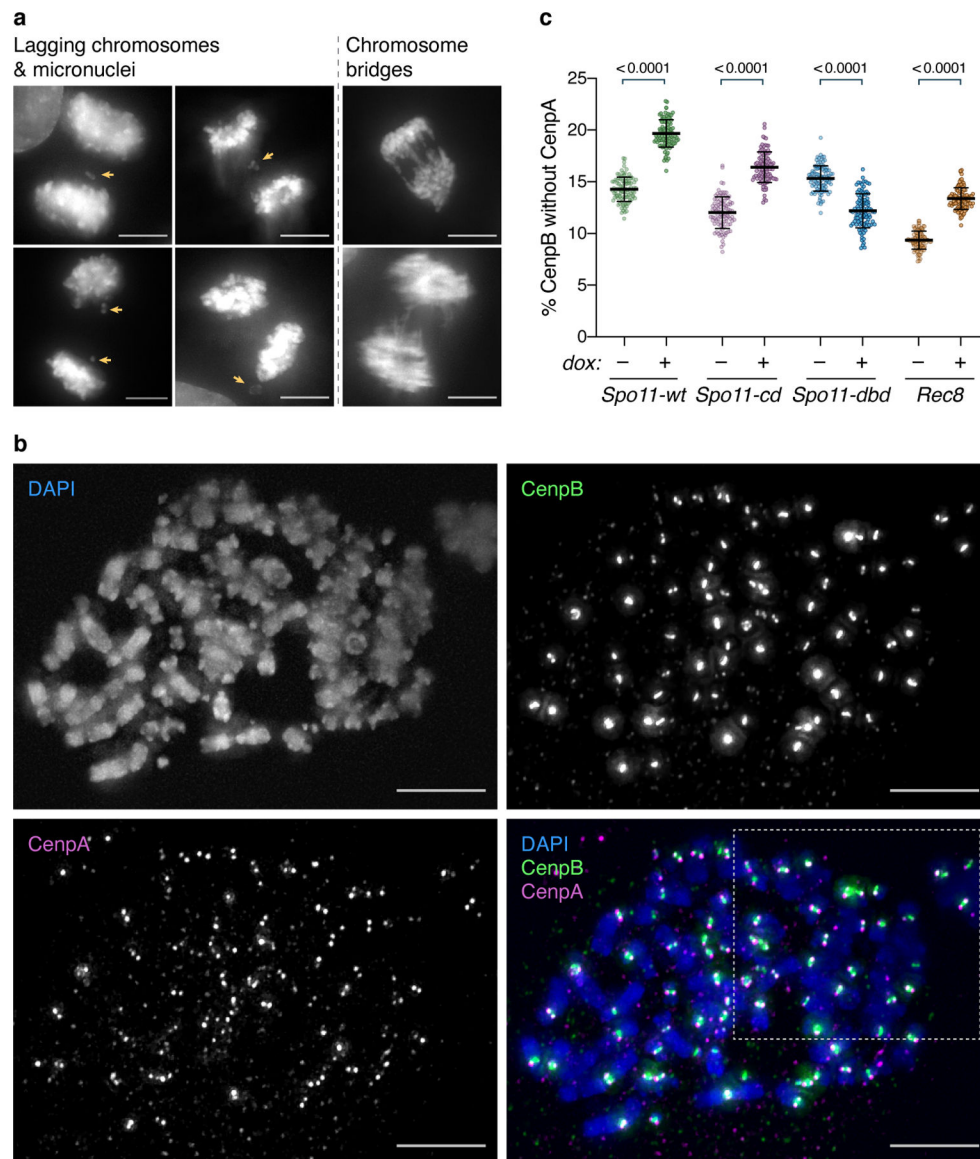
Extended Data Fig. 9. U2OS cells expressing Spo11 alleles and Rec8 show centromeric and mitotic defects.
(a) Additional images of mitoses scored for segregation defects. Chromosomes are counterstained with DAPI. Examples of lagging chromosomes or micronuclei are indicated by yellow arrows. Scale bars = 10 μm. (b) Individual channels from representative image of metaphase chromosome spreads from Fig. 5c, in grayscale. KTs are stained for CenpB (green) and CenpA (magenta); chromosomes are counterstained with DAPI. Scale bar = 10 μm. (c) Data for KT loss (Fig. 5d) bootstrapped as described in Methods to generate 100 estimates of %CenpB half-bars (centromeres) without CenpA per sample. Mean ± standard

deviation bars are superimposed on individual data points. p values indicated above brackets are calculated by an ordinary one-way ANOVA and Sidak's multiple comparison test (for each genotype ±dox). The data show low variability between samples of the same genotype from different experiments, justifying pooling of data from independent experiments; statistically significant differences in means are seen upon doxycycline induction.
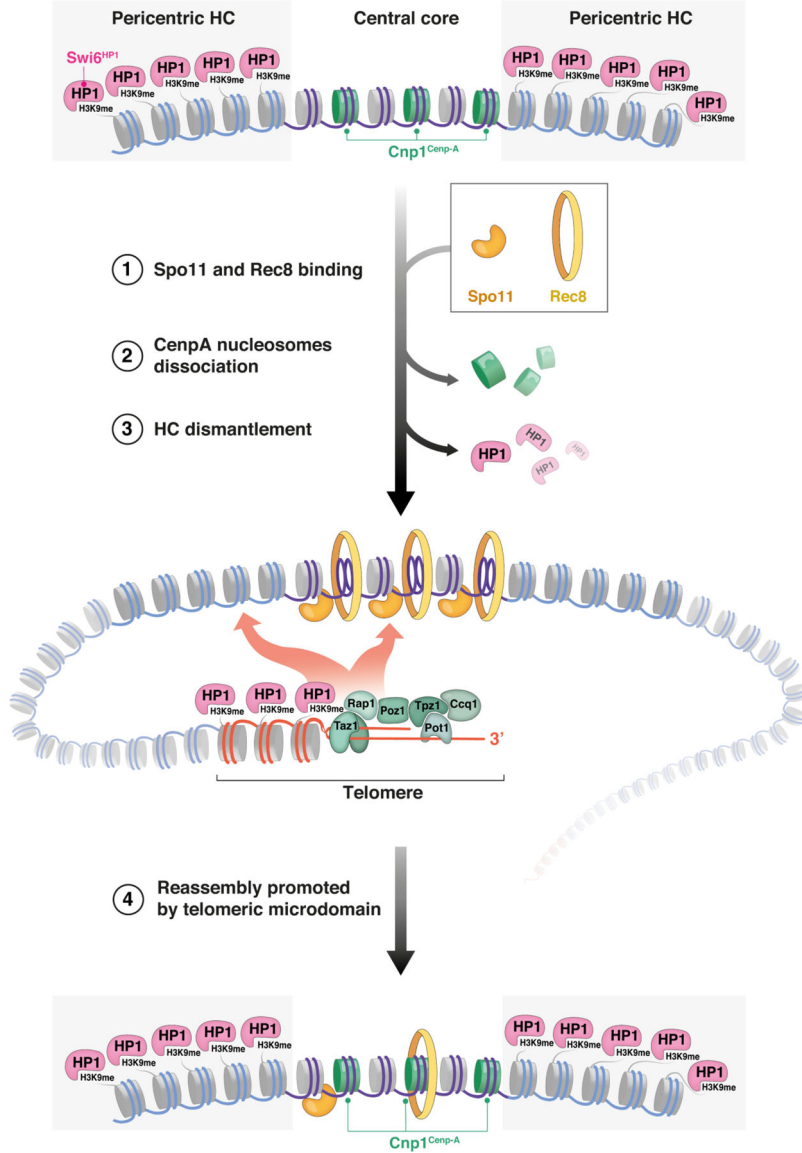
Extended Data Fig. 10. Working model for centromere dismantlement in meiosis.
Meiotic Spo11 and Rec8 binding to chromatin (1) destabilizes CenpA nucleosomes; (2) their dismantlement propagates outwards to surrounding pericentric HC (3). (4) Telomeres, which are in close proximity to centromeres during bouquet formation in meiotic prophase, provide a microdomain that favors centromeric reassembly.

Supplementary Material

Refer to Web version on PubMed Central for supplementary material.

Acknowledgements

References

1. Klutstein M, Fennell A, Fernandez-Alvarez A & Cooper JP The telomere bouquet regulates meiotic centromere assembly. Nat Cell Biol 17, 458–469 (2015). [PubMed: 25774833]

2. Allshire RC & Karpen GH Epigenetic regulation of centromeric chromatin: old dogs, new tricks? Nat Rev Genet 9, 923–937 (2008). [PubMed: 19002142]

3. McKinley KL & Cheeseman IM The molecular basis for centromere identity and function. Nat Rev Mol Cell Biol 17, 16–29 (2016). [PubMed: 26601620]

4. Allshire RC, Javerzat JP, Redhead NJ & Cranston G Position effect variegation at fission yeast centromeres. Cell 76, 157–169 (1994). [PubMed: 8287474]

5. Cam HP et al. Comprehensive analysis of heterochromatin- and RNAi-mediated epigenetic control of the fission yeast genome. Nat Genet 37, 809–819 (2005). [PubMed: 15976807]

6. Folco HD, Pidoux AL, Urano T & Allshire RC Heterochromatin and RNAi are required to establish CENP-A chromatin at centromeres. Science 319, 94–97 (2008). [PubMed: 18174443]

7. de Lange T Shelterin-Mediated Telomere Protection. Annu Rev Genet 52, 223–247 (2018). [PubMed: 30208292]

8. Hou H & Cooper JP Stretching, scrambling, piercing and entangling: Challenges for telomeres in mitotic and meiotic chromosome segregation. Differentiation 100, 12–20 (2018). [PubMed: 29413748]

9. Kanoh J, Sadaie M, Urano T & Ishikawa F Telomere binding protein Taz1 establishes Swi6 heterochromatin independently of RNAi at telomeres. Curr Biol 15, 1808–1819 (2005). [PubMed: 16243027]

10. Barchi M, Cohen P & Keeney S Special issue on "recent advances in meiotic chromosome structure, recombination and segregation". Chromosoma 125, 173–175 (2016). [PubMed: 27022980]

11. Robert T et al. The TopoVIB-Like protein family is required for meiotic DNA double-strand break formation. Science 351, 943–949 (2016). [PubMed: 26917764]

12. Vrielynck N et al. A DNA topoisomerase VI-like complex initiates meiotic recombination. Science 351, 939–943 (2016). [PubMed: 26917763]

13. Klutstein M & Cooper JP The Chromosomal Courtship Dance-homolog pairing in early meiosis. Curr Opin Cell Biol 26C, 123–131 (2014).

14. Kitajima TS, Yokobayashi S, Yamamoto M & Watanabe Y Distinct cohesin complexes organize meiotic chromosome domains. Science 300, 1152–1155 (2003). [PubMed: 12750522]

15. Duro E & Marston AL From equator to pole: splitting chromosomes in mitosis and meiosis. Genes Dev 29, 109–122 (2015). [PubMed: 25593304]

16. Kitajima TS, Kawashima SA & Watanabe Y The conserved kinetochore protein shugoshin protects centromeric cohesion during meiosis. Nature 427, 510–517 (2004). [PubMed: 14730319]

17. Chikashige Y et al. Telomere-led premeiotic chromosome movement in fission yeast. Science 264, 270–273 (1994). [PubMed: 8146661]

18. Cooper JP, Watanabe Y & Nurse P Fission yeast Taz1 protein is required for meiotic telomere clustering and recombination. Nature 392, 828–831 (1998). [PubMed: 9572143]

19. Nimmo ER, Pidoux AL, Perry PE & Allshire RC Defective meiosis in telomere-silencing mutants of Schizosaccharomyces pombe. Nature 392, 825–828 (1998). [PubMed: 9572142]

20. Scherthan H A bouquet makes ends meet. Nat Rev Mol Cell Biol 2, 621–627 (2001). [PubMed: 11483995]

21. Fennell A, Fernandez-Alvarez A, Tomita K & Cooper JP Telomeres and centromeres have interchangeable roles in promoting meiotic spindle formation. J Cell Biol 208, 415–428 (2015). [PubMed: 25688135]

22. Sharif WD, Glick GG, Davidson MK & Wahls WP Distinct functions of S. pombe Rec12 (Spo11) protein and Rec12-dependent crossover recombination (chiasmata) in meiosis I; and a requirement for Rec12 in meiosis II. Cell Chromosome 1, 1 (2002). [PubMed: 12437782]

23. Nichols MD, DeAngelis K, Keck JL & Berger JM Structure and function of an archaeal topoisomerase VI subunit with homology to the meiotic recombination factor Spo11. EMBO J 18, 6177–6188 (1999). [PubMed: 10545127]

24. Diaz RL, Alcid AD, Berger JM & Keeney S Identification of residues in yeast Spo11p critical for meiotic DNA double-strand break formation. Mol Cell Biol 22 (2002).

25. Miyoshi T et al. A central coupler for recombination initiation linking chromosome architecture to S phase checkpoint. Mol Cell 47, 722–733 (2012). [PubMed: 22841486]

26. Fowler KR, Gutierrez-Velasco S, Martin-Castellanos C & Smith GR Protein determinants of meiotic DNA break hot spots. Mol Cell 49, 983–996 (2013). [PubMed: 23395004]

27. Nonaka N et al. Recruitment of cohesin to heterochromatic regions by Swi6/HP1 in fission yeast. Nat Cell Biol 4, 89–93 (2002). [PubMed: 11780129]

28. Kugou K et al. Rec8 guides canonical Spo11 distribution along yeast meiotic chromosomes. Mol Biol Cell 20, 3064–3076 (2009). [PubMed: 19439448]

29. Lopez-Serra L, Kelly G, Patel H, Stewart A & Uhlmann F The Scc2-Scc4 complex acts in sister chromatid cohesion and transcriptional regulation by maintaining nucleosome-free regions. Nat Genet 46, 1147–1151 (2014). [PubMed: 25173104]

30. Munoz S, Minamino M, Casas-Delucchi CS, Patel H & Uhlmann F A Role for Chromatin Remodeling in Cohesin Loading onto Chromosomes. Mol Cell 74, 664–673 e665 (2019). [PubMed: 30922844]

31. Pointner J et al. CHD1 remodelers regulate nucleosome spacing in vitro and align nucleosomal arrays over gene coding regions in S. pombe. EMBO J 31, 4388–4403 (2012). [PubMed: 23103765]

32. Shim YS et al. Hrp3 controls nucleosome positioning to suppress non-coding transcription in eu- and heterochromatin. EMBO J 31, 4375–4387 (2012). [PubMed: 22990236]

33. Hennig BP, Bendrin K, Zhou Y & Fischer T Chd1 chromatin remodelers maintain nucleosome organization and repress cryptic transcription. EMBO reports 13, 997–1003 (2012). [PubMed: 23032292]

34. Folco HD et al. Untimely expression of gametogenic genes in vegetative cells causes uniparental disomy. Nature 543, 126–130 (2017). [PubMed: 28199302]

35. Harigaya Y et al. Selective elimination of messenger RNA prevents an incidence of untimely meiosis. Nature 442, 45–50 (2006). [PubMed: 16823445]

36. Sugiyama T & Sugioka-Sugiyama R Red1 promotes the elimination of meiosis-specific mRNAs in vegetatively growing fission yeast. EMBO J 30, 1027–1039 (2011). [PubMed: 21317872]

37. Lu M & He X Intricate regulation on epigenetic stability of the subtelomeric heterochromatin and the centromeric chromatin in fission yeast. Current genetics 65, 381–386 (2019). [PubMed: 30244281]

38. Lindsey SF et al. Potential role of meiosis proteins in melanoma chromosomal instability. Journal of skin cancer 2013, 190109 (2013). [PubMed: 23840955]

39. Koslowski M et al. Multiple splice variants of lactate dehydrogenase C selectively expressed in human cancer. Cancer research 62, 6750–6755 (2002). [PubMed: 12438276]

40. Cho NW, Dilley RL, Lampson MA & Greenberg RA Interchromosomal homology searches drive directional ALT telomere movement and synapsis. Cell 159, 108–121 (2014). [PubMed: 25259924]

41. McKinley KL et al. The CENP-L-N Complex Forms a Critical Node in an Integrated Meshwork of Interactions at the Centromere-Kinetochore Interface. Mol Cell 60, 886–898 (2015). [PubMed: 26698661]

42. Boateng KA, Bellani MA, Gregoretti IV, Pratto F & Camerini-Otero RD Homologous pairing preceding SPO11-mediated double-strand breaks in mice. Dev Cell 24, 196–205 (2013). [PubMed: 23318132]

43. DeWall KM, Davidson MK, Sharif WD, Wiley CA & Wahls WP A DNA binding motif of meiotic recombinase Rec12 (Spo11) defined by essential glycine-202, and persistence of Rec12 protein after completion of recombination. Gene 356, 77–84 (2005). [PubMed: 16009511]

44. Masumoto H, Masukata H, Muro Y, Nozaki N & Okazaki T A human centromere antigen (CENP-B) interacts with a short specific sequence in alphoid DNA, a human centromeric satellite. J Cell Biol 109, 1963–1973 (1989). [PubMed: 2808515]

45. Fachinetti D et al. A two-step mechanism for epigenetic specification of centromere identity and function. Nat Cell Biol 15, 1056–1066 (2013). [PubMed: 23873148]

46. Hoffmann S et al. CENP-A Is Dispensable for Mitotic Centromere Function after Initial Centromere/Kinetochore Assembly. Cell reports 17, 2394–2404 (2016). [PubMed: 27880912]

47. Cooke CA, Bernat RL & Earnshaw WC CENP-B: a major human centromere protein located beneath the kinetochore. J Cell Biol 110, 1475–1488 (1990). [PubMed: 2335558]

48. Bayani J et al. Spectral karyotyping identifies recurrent complex rearrangements of chromosomes 8, 17, and 20 in osteosarcomas. Genes Chromosomes Cancer 36, 7–16 (2003). [PubMed: 12461745]

49. Bakhoum SF, Thompson SL, Manning AL & Compton DA Genome stability is ensured by temporal control of kinetochore-microtubule dynamics. Nat Cell Biol 11, 27–35 (2009). [PubMed: 19060894]

50. Gruhn JR et al. Chromosome errors in human eggs shape natural fertility over reproductive life span. Science 365, 1466–1469 (2019). [PubMed: 31604276]

51. Zielinska AP et al. Meiotic Kinetochores Fragment into Multiple Lobes upon Cohesin Loss in Aging Eggs. Curr Biol 29, 3749–3765 e3747 (2019). [PubMed: 31679939]

52. Jansen LE, Black BE, Foltz DR & Cleveland DW Propagation of centromeric chromatin requires exit from mitosis. J Cell Biol 176, 795–805 (2007). [PubMed: 17339380]

53. Smoak EM, Stein P, Schultz RM, Lampson MA & Black BE Long-Term Retention of CENP-A Nucleosomes in Mammalian Oocytes Underpins Transgenerational Inheritance of Centromere Identity. Curr Biol 26, 1110–1116 (2016). [PubMed: 27040782]

54. Swartz SZ et al. Quiescent Cells Actively Replenish CENP-A Nucleosomes to Maintain Centromere Identity and Proliferative Potential. Dev Cell 51, 25–48 (2019).

55. Liebelt F et al. The poly-SUMO2/3 protease SENP6 enables assembly of the constitutive centromere-associated network by group deSUMOylation. Nat Commun 10, 3987 (2019). [PubMed: 31485003]

56. Mitra S et al. Genetic screening identifies a SUMO protease dynamically maintaining centromeric chromatin. Nat Commun 11, 501 (2020). [PubMed: 31980633]

57. Miller MP, Unal E, Brar GA & Amon A Meiosis I chromosome segregation is established through regulation of microtubule-kinetochore interactions. Elife 1, e00117 (2012). [PubMed: 23275833]

58. Zhang W et al. Centromere and kinetochore gene misexpression predicts cancer patient survival and response to radiotherapy and chemotherapy. Nat Commun 7, 12619 (2016). [PubMed: 27577169]

59. Bahler J et al. Heterologous modules for efficient and versatile PCR-based gene targeting in Schizosaccharomyces pombe. Yeast 14, 943–951 (1998). [PubMed: 9717240]

60. Fennell A, Fernandez-Alvarez A, Tomita K & Cooper JP Telomeres and centromeres have interchangeable roles in promoting meiotic spindle formation. J Cell Biol 208, 415–428 (2015). [PubMed: 25688135]

61. Fernandez-Alvarez A, Bez C, O'Toole ET, Morphew M & Cooper JP Mitotic Nuclear Envelope Breakdown and Spindle Nucleation Are Controlled by Interphase Contacts between Centromeres and the Nuclear Envelope. Dev Cell 39, 544–559 (2016). [PubMed: 27889481]

62. Tomita K & Cooper JP The telomere bouquet controls the meiotic spindle. Cell 130, 113–126 (2007). [PubMed: 17632059]

63. McKinley KL et al. The CENP-L-N Complex Forms a Critical Node in an Integrated Meshwork of Interactions at the Centromere-Kinetochore Interface. Mol Cell 60, 886–898 (2015). [PubMed: 26698661]

64. Kyriacou E & Heun P High-resolution mapping of centromeric protein association using APEX-chromatin fibers. Epigenetics Chromatin 11, 68 (2018). [PubMed: 30445992]

65. Hou H et al. Histone variant H2A.Z regulates centromere silencing and chromosome segregation in fission yeast. J Biol Chem 285, 1909–1918 (2010). [PubMed: 19910462]

66. Bellani MA, Boateng KA, McLeod D & Camerini-Otero RD The expression profile of the major mouse SPO11 isoforms indicates that SPO11beta introduces double strand breaks and suggests that SPO11alpha has an additional role in prophase in both spermatocytes and oocytes. Mol Cell Biol 30, 4391–4403 (2010). [PubMed: 20647542]
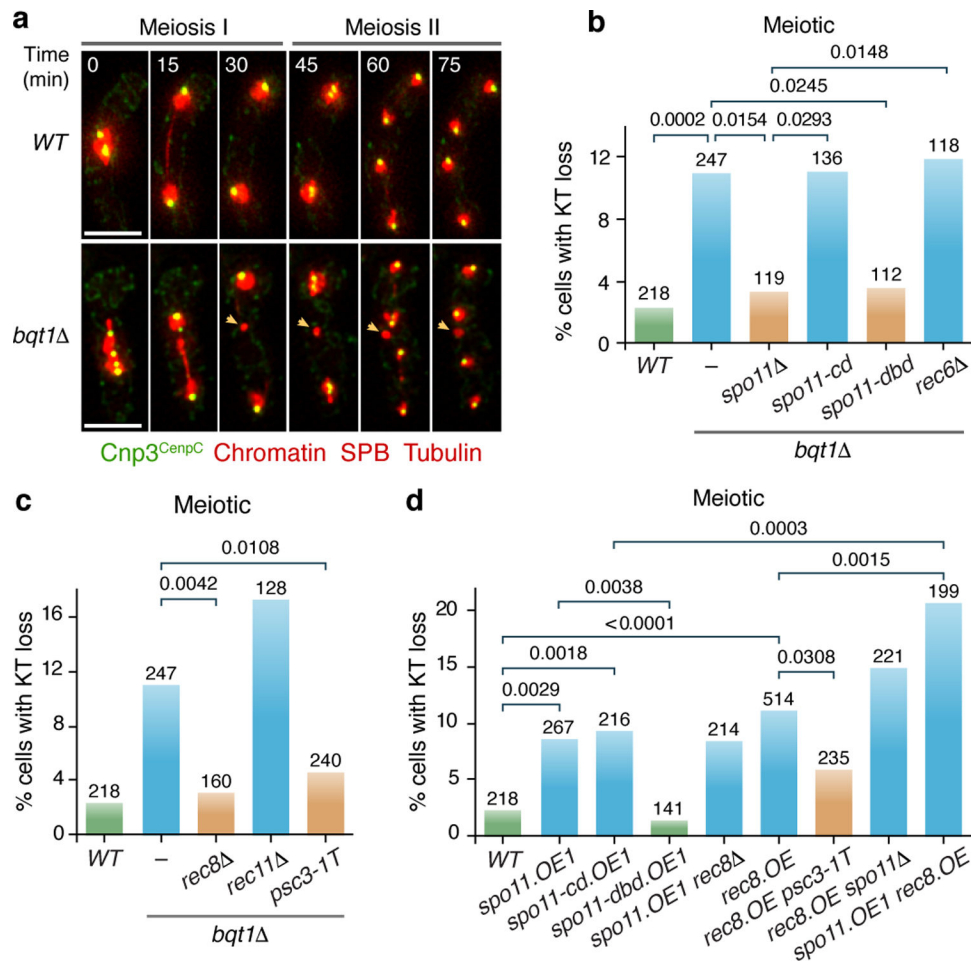
Fig. 1. Spo11 and Rec8 cause KT loss.
(a) Representative films of KT loss. KTs (Cnp3^{CenpC}-GFP), chromatin (Pht1^{H2AZ}-mCherry), SPBs (Sid4-mCherry), and microtubules (mCherry-Atb2) are visualized. t = 0 is the first frame in MI. Arrows indicate unsegregated chromosomes lacking KTs. Scale bars = 5μm. (b-d) Quantitation of KT loss as in (a). (b) *spo11Δ* or *-dbd* rescue *bqt1Δ* KT loss; *spo11-cd* or *rec6Δ* do not. (c) *rec8Δ* and *psc3–1T* suppress KT loss while *rec11Δ* does not. (d) Overexpression of *spo11* (*spo11.OE1* controlled by *nmt41* promoter) or *rec8* (*rec8.OE* controlled by *adh1* promoter) elevates KT loss rate and overwhelms bouquet-mediated KT reassembly. The effect of overexpressing Spo11 depends on DNA binding but not catalytic activity or Rec8. KT loss upon Rec8 overexpression is suppressed by *psc3–1T* but not *spo11Δ*. Total number of films analyzed is indicated above each bar. p values, determined by two-tailed Fisher's exact tests, are indicated above brackets; the number of experimental repeats for all figures is given in Table S1.
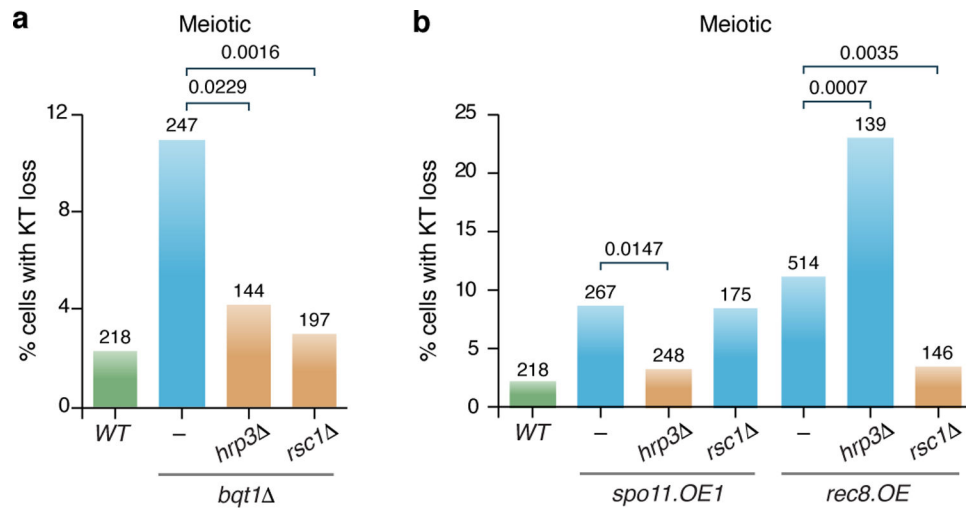
Fig. 2. Spo11 and Rec8 require the CHD or RSC chromatin remodelers, respectively, to dismantle meiotic KTs.

Quantitation of KT loss as in Figure 1a. (a) Deletion of *hrp3+* or *rsc1+* suppresses KT loss in the absence of the bouquet. (b) *rsc1Δ* or *hrp3Δ* specifically reverse KT loss caused by Rec8 or Spo11 overexpression, respectively. Total number of films analyzed is indicated above each bar. p values, determined by two-tailed Fisher's exact tests, are indicated above brackets.
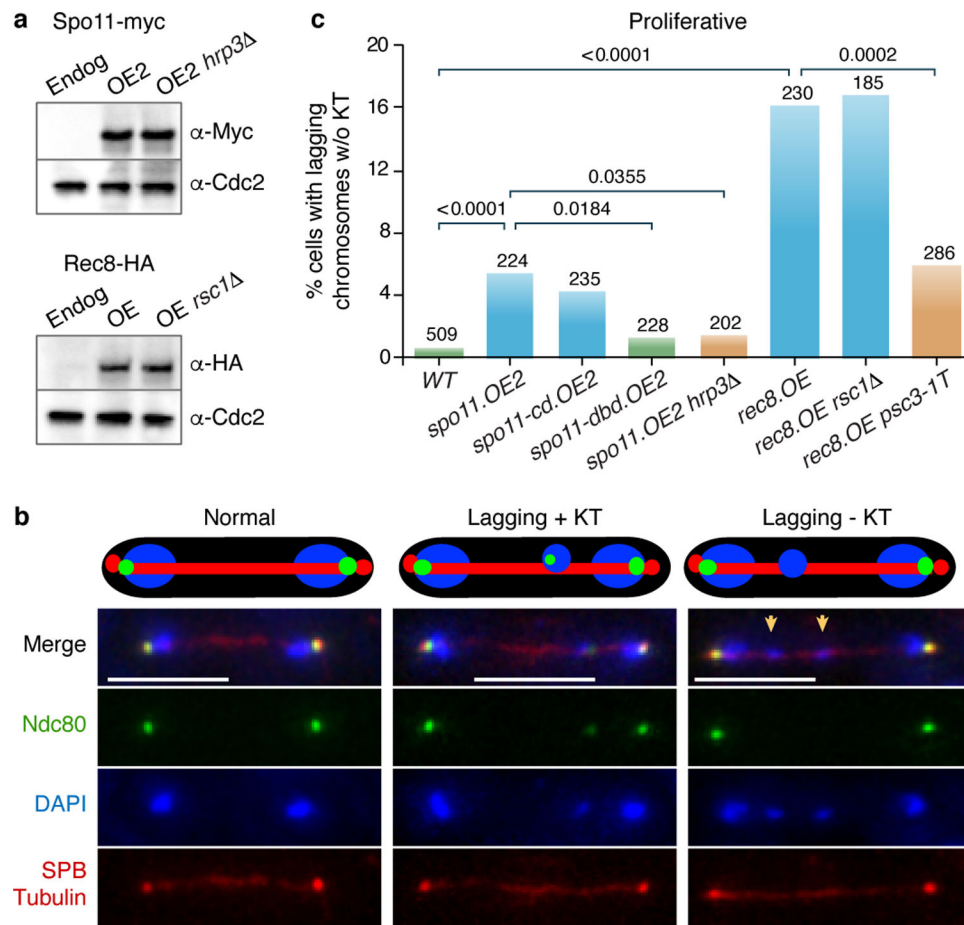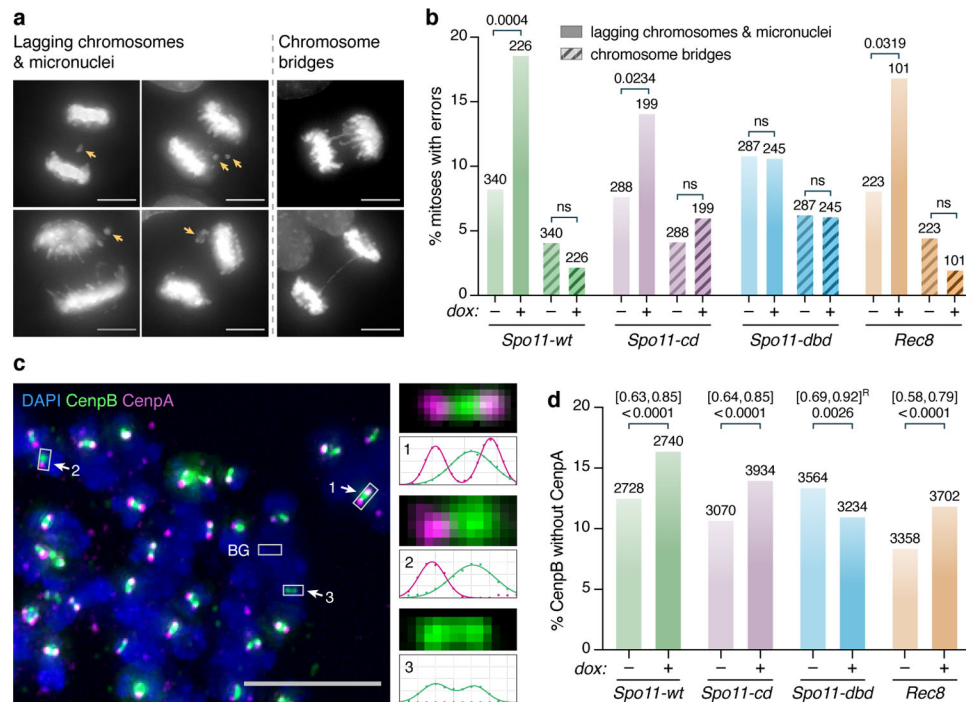
Fig. 3. Expression of Spo11 or Rec8 in proliferating cells causes KT loss.

(a) Western blots show no detectable expression of endogenously (Endo) 13xmyc-tagged Spo11 or 3xHA-tagged Rec8, but strong expression when under control of the *adh1* promoter. Expression levels do not change upon *hrp3+* or *rsc1+* deletion. anti-Cdc2 provides loading control. Representative images of 3 repeats are shown.

(b) KT loss in proliferating anaphase cells. Snapshots of fixed cells in late anaphase: KT (Ndc80–2xGFP), chromatin (DAPI, 4′,6-diamidino-2-phenylindole), SPB (Sid4-mCherry), and spindle (mCherry-Atb2$^{\alpha\text{-Tubulin}}$) are visualized. Lagging chromosomes lacking KT are indicated by arrows. Lagging chromosomes with intact KT are excluded from quantitation. Scale bars = 5μm.

(c) Quantitation of KT loss as in (b). Expression of Spo11 elevates KT loss rate; this is reversed by *hrp3+* deletion. Spo11-cd, but not Spo11-dbd, confers mitotic KT loss. Rec8 expression increases mitotic KT loss; this is reversed by *psc3–1T* but not by *rsc1*. Total number of films analyzed is indicated above each bar. p values, determined by two-tailed Fisher's exact tests, are indicated above brackets.

Fig. 4. Expression of Spo11 or Rec8 reduces overall level of centromere bound Cnp1^{CenpA}.
(a) Diagram of centromeric chromatin. Outer and inner KTs are built upon Cnp1^{CenpA} nucleosomes at the central core, which is flanked by pericentric HC.
(b-c) ChIP analysis of Cnp1^{CenpA} (b) and H3K9me2 (c) at centromeric central core. Ectopic Cnp1^{CenpA}-GFP or H3K9me2 were immunoprecipitated with antibody against GFP or H3K9me2 and analyzed by qPCR. Enrichment levels at the central core were normalized against that of *act1*, and then with that of (b) a *wt* strain with no Cnp1^{CenpA} tag, or (c) *clr4* cells lacking H3K9me2. Each grey dot represents a biological replicate. Bars represent mean enrichment, and error bars the standard deviation.

Fig. 5. Spo11 and Rec8 expression in human cells compromises centromeres.

(a) Representative images of mitoses scored for missegregating chromosomes, examples of which are indicated by yellow arrows. Scale bars = 10 μm.

(b) Quantitation of chromosome segregation defects. Expression of Spo11-wt, Spo11-cd or Rec8, but not Spo11-dbd, increases the frequency of lagging chromosomes and micronuclei; chromosome bridge frequency remains unchanged in all cases. The total number of mitoses analyzed in 4 (*Spo11*) or 3 (*Rec8*) experiments is indicated above each bar. p values, determined by two-tailed Fisher's exact tests, are indicated above brackets. ns: not significant.

(c) Representative image of metaphase chromosome spreads. KTs are stained for CenpB and CenpA; chromosomes with DAPI. Numbered arrowheads indicate boxed regions magnified alongside with automated Gaussian fits to CenpA/B intensity profiles (see Methods) and illustrate CenpA staining patterns: (1) two dots, (2) one-sided loss, or (3) complete loss of CenpA from the KT. Scale bars = 10 μm. See Extended Data Fig. 9b for single channels. BG indicates a representative region used for background subtraction. (d) Automated quantitation (see Methods) of KT loss on metaphase spreads as scored *via* centromeres lacking CenpA at one or both ends. Expression of Spo11, Spo11-cd or Rec8, but not Spo11-dbd, increases the KT loss rate. The total number of KTs analyzed over 3 experiments is indicated above each bar. p values, determined by two-tailed Fisher's exact tests, are indicated above brackets. 95% confidence intervals of the odds ratio or its reciprocal (*Spo11-dbd*) are indicated in square brackets.